Dynamically correlated gas under resetting: exact results for general resetting protocols

Master's thesis

Supervisor:
Prof. Alessandro Pelizzola
Prof. Satya Majumdar

Candidate:
Gabriele de Mauro

Academic Year 2024–2025

Abstract

In this thesis, we consider a one-dimensional gas of N independent Brownian particles subject to stochastic resetting, with inter-reset times drawn from a general waiting-time distribution $\psi(\tau)$. This includes the well-known Poissonian case, where $\psi(\tau) = re^{-r\tau}$, and extends to more general classes of resetting, such as heavy-tailed and bounded distributions. While our study is focused on the one-dimensional case, the main results are easily generalizable to higher dimensions. Exploiting the renewal structure of the resetting dynamics, we derive explicit analytical expressions for the non-equilibrium stationary state (NESS) and various observables of interest, including particle density, extreme value statistics, order statistics, gap statistics, and full counting statistics. We demonstrate that these observables take a scaling form that exhibits some universal scaling behaviors, characterized by scale factors independent of the specific resetting protocol. However, their detailed forms depend explicitly on the distribution of inter-reset times. Remarkably, we identify a novel class of extreme value statistics (EVS) not previously described in the literature. We classify the resetting protocols into three distinct universality classes based on the tail behavior of the resetting-time distribution: exponential decay, bounded support, and power-law tails. Our theoretical predictions are supported by numerical simulations. These results extend the understanding of resetting dynamics in many-body systems and offer new insights into non-equilibrium systems with strongly correlated degrees of freedom.

Contents

Introduction

It is quite common in everyday life for certain processes to be interrupted at random times and then restarted from a fixed initial condition. For example, when looking for misplaced keys at home, people often return repeatedly to a known starting point (e.g., the entryway or a specific room) to restart their search if the keys aren't found within a reasonable timeframe. Similarly, during a visual search in a crowded place, our gaze tends to return to the center of the visual field before resuming the search when the target is not immediately found.

A prototypical example of such processes, known as stochastic resetting, was introduced in [1], where a diffusive particle is reset to its initial position at a constant rate r. Since then, stochastic resetting has been studied in a wide variety of contexts. In particular, it has found applications in many search problems [2–15], where it can, under certain conditions, improve search efficiency. Resetting has also been employed in computer simulations [16] to improve sampling efficiency in molecular dynamics algorithms, as it helps the system to escape bad local minima. More generally, incorporating a resetting mechanism into stochastic algorithms may help them avoid getting stuck before completing their execution [17–21]. In biology, stochastic resetting is used to model RNA synthesis, where transcription is stochastically interrupted via backtracking [22, 23]. Resetting the dynamics of a physical system has profound effects on it: the resetting mechanism breaks detailed balance and typically drives the system into a non-equilibrium stationary state (NESS). In general, non-equilibrium systems remain poorly understood, and stochastic resetting offers a valuable framework for constructing broad classes of such systems where the stationary state can be computed explicitly. This makes it a powerful tool for gaining deeper insights into the behavior of systems far from equilibrium. The implications of this mechanism have been extensively explored in single-particle systems, such as Lévy walks, Lévy flights, and run-and-tumble particles [24–27]. Analytical predictions from resetting systems have also been verified experimentally using colloidal particles in harmonic traps [28–31]. The same applies to quantum systems, where resetting is realized as a unitary evolution interrupted by random resets to the initial state [32–35]. Moreover, the *single-particle* problem has been generalized to arbitrary waiting time distributions $\psi(\tau)$ between resets [36], including power-law distributions [37] and time-dependent resetting rates $r(t)$ [15]. A general master equation for such systems was formulated in [38].

The influence of stochastic resetting has also been studied in systems with many degrees of freedom (DOF) [39–43]. Its effects become particularly intriguing when all DOF are reset simultaneously. For example, in a one-dimensional gas of Brownian searchers [39], although the particles evolve independently between resets, the act of resetting all particles at once induces dynamically emergent long-range correlations. Remarkably, despite the presence of strong correlations and the non-equilibrium nature of the steady state, many observables of interest remain analytically tractable [40].

These include:

- **the average density of particles**;
- **the extreme value statistics (EVS)**, which refer to the distribution of the maximum or minimum value among a set of random variables (which in this case are the particles' positions on the real line);
- **the order statistics**, which focus on the relative ordering of all particles;
- **the gap statistics**, which study the spacing between consecutive particles;
- **the full counting statistics (FCS)**, which count how many particles out of the total N lie within a symmetric interval $[-L, L]$ centered at the origin.

The possibility to analytically calculate all these quantities is a very rare feature for non-equilibrium systems.

Among all these observables, the study of EVS is of particular interest. While the classical theory of EVS classifies the distribution of the maximum of independent and identically distributed (i.i.d) variables into Gumbel, Fréchet, and Weibull [44, 45] universality classes, much less is known in the presence of strong correlations. Some generalisations have been obtained for weakly correlated variables [46, 47], or non identically distributed random variables [48], but for strongly correlated variables we do not have general results and only a few cases have been solved [46, 49]. Resetting provides a rare example where such statistics can still be computed exactly, even in the correlated regime.

As discussed above, previous studies have considered many-body systems under *constant-resetting rate* r, or more general resetting protocols $\psi(\tau)$ in the *single-particle case*. In contrast, this thesis extends the study of *arbitrary resetting protocols* to a *many-body setting*. We focus on a one-dimensional gas of N independent Brownian particles, where all particles are reset simultaneously to their initial positions at random times drawn from a general distribution $\psi(\tau)$. We first recover known results in the Poissonian case, where $\psi(\tau) = re^{-r\tau}$, and then investigate the stationary state for two non-Poissonian examples: a power-law and a bounded distribution. We then find exact results for general classes of resetting protocols. This analysis allows us to identify which features of the non-equilibrium stationary state (NESS) are universal and which depend sensitively on the specific form of $\psi(\tau)$.

A natural framework to approach this problem is that of conditionally independent and identically distributed (c.i.i.d.) variables [40], which we introduce in Section 2.1.1. In this setting, independent samples drawn from a distribution with a shared random parameter become correlated once we average over that parameter. This framework arises naturally in many models and, in our case, gives rise to non-trivial correlations in the stationary state after the common parameter is integrated out.

Chapter 1

Poissonian stochastic resetting

In this chapter, we introduce the paradigmatic example of a single diffusing particle that undergoes Poissonian stochastic resetting. We then generalize the analysis to a system of N independent particles, which are all reset simultaneously. Despite the absence of interactions between the particles during their diffusive motion, the global resetting introduces correlations that persist in the stationary state. These correlations are of particular interest, as they emerge purely from the resetting protocol and not from direct interactions.

1.1 One diffusing particle

We consider a single particle in one dimension, whose position is indicated by $x(t)$, which diffuses with diffusion constant D. We indicate with $p(x,t|x_0)$ the probability density function (PDF) that the particle is at position x at time t, having started at x_0 at time $t=0$. This PDF evolves in time with the Fokker-Planck equation given by:

$$\frac{\partial p(x,t \mid x_0)}{\partial t} = D\frac{\partial^2 p(x,t \mid x_0)}{\partial x^2} \tag{1.1}$$

with initial condition $p(x,t=0|x_0) = \delta(x-x_0)$. The solution of this equation on the full real line is given by

$$p(x,t \mid x_0) = \frac{1}{\sqrt{4\pi D t}} \exp\left(-\frac{(x-x_0)^2}{4Dt}\right) \tag{1.2}$$

We now consider the case in which the same diffusing particle is stochastically reset to the initial condition with a constant resetting rate r. If we discretise time into small intervals of size dt, the position of the particle evolves according to the following stochastic rule:

$$x(t+dt) = \begin{cases} 0 & \text{with probability } r\,dt, \\ x(t) + \sqrt{2D\,dt}\,\eta(t) & \text{with probability } 1-r\,dt, \end{cases} \tag{1.3}$$

where $\eta(t)$ is a Gaussian random variables with zero mean and unit variance.

Although one could solve this problem by generalizing Eq. (1.1), it is more insightful for our purpose to exploit the underlying *renewal structure* of the dynamics. Indeed, each time a reset occurs, the process restarts from the initial condition, rendering the prior history irrelevant. Consequently, the state of the system at any given time t depends solely on the time elapsed

since the last reset (see Figure 2.1). This framework is particularly effective for determining the stationary state and for generalizing to systems with many particles and non-exponential resetting protocols.

Under this approach, the probability density function $p_r(x, t \mid x_0)$ in the presence of resetting at rate r can be expressed as the sum of two contributions given by:

$$p_r(x, t \mid x_0) = e^{-rt}\, p(x, t \mid x_0) + r \int_0^t d\tau\, e^{-r\tau}\, p(x, \tau \mid x_0). \tag{1.4}$$

The first term corresponds to the trajectories for which no resetting has occurred up to time t, which happens with probability e^{-rt}; in this case, the PDF is simply that of the process without resetting $p(x, t|x_0)$. The second term accounts for trajectories where at least one resetting as occurred. In this case, we consider that the *last* reset occurred at time $t - \tau$, after which the particle evolved freely for a time τ (see Figure 2.1).

The stationary state is then attained in the limit $t \to \infty$, where the first term in eq. (1.4) vanishes, leading to

$$p_r^*(x|x_0) = p_r(x, t \to \infty|x_0) = r \int_0^\infty d\tau\, e^{-r\tau}\, p(x, \tau|x_0) \tag{1.5}$$

The above integral can be explicitly solved giving:

$$p_r^*(x|x_0) = \frac{1}{2}\sqrt{\frac{r}{D}}\, \exp\left(-\sqrt{\frac{r}{D}}\, |x - x_0|\right) \tag{1.6}$$

This PDF has a cusp at the resetting position and decays exponentially on both sides. Since the resetting move breaks detailed balance, eq. (1.6) corresponds to a NESS.

1.2 Many diffusing particles

We now extend the single-particle model to a system with many degrees of freedom. Specifically, we consider a one-dimensional gas of N non-interacting Brownian particles, each diffusing independently along the real line with diffusion constant D. At random times, with constant rate r, all particles are simultaneously reset to a fixed position, which we take to be the origin without loss of generality. This model, first introduced in [39], provides a minimal yet rich framework to study non-equilibrium behavior in many-body systems subject to resetting.

Between two consecutive resets, the positions of the particles evolve independently according to free diffusion. If we denote by $\vec{x} = \{x_1, \ldots, x_N\}$ the positions of the particles , the joint probability density function (JPDF) in the absence of resetting is given by the product of Gaussian propagators:

$$\mathcal{G}_0(\vec{x}, t) = \prod_{i=1}^{N} \frac{1}{\sqrt{4\pi D t}} \exp\left(-\frac{x_i^2}{4Dt}\right). \tag{1.7}$$

As in the one-particle example, we consider that a resetting event happens with a constant rate r. This means that we think of discretising time into small intervals of duration dt; at each time step, either a reset occurs with probability $r\, dt$, bringing all particles back to the origin, or the particles continue their Brownian motion with probability $1 - r\, dt$. This construction

implies that the waiting times τ between resets are independent and exponentially distributed with PDF:

$$\psi(\tau) = re^{-r\tau}.$$

In Chapter 2, we generalize $\psi(\tau)$ to arbitrary waiting time distributions. This generalization constitutes the main result of this work. Although the particles evolve independently between resets, the fact that they are all reset simultaneously introduces strong correlations in the system, as it can be seen in (1.9) and in (2.22).

The JPDF $\mathcal{P}_r(\vec{x}, t)$, representing the probability density of finding particles at positions $\vec{x}$ at time t under a constant resetting rate r, can be derived explicitly by exploiting the renewal structure of the process, as we have already done for the single particle case. We avoid indicating that all particles start from the origin, which is also the resetting position. As in the single-particle case, we make use of the renewal property of the dynamics, since each reset brings the system back to its initial condition, making its previous trajectory irrelevant. As a result, we can divide all trajectories into two groups: those in which no resetting occurs up to time t, and those in which at least one reset takes place before t. The JPDF can thus be expressed as the sum of two distinct contributions:

$$\mathcal{P}_r(\vec{x}, t) = e^{-rt}\mathcal{G}_0(\vec{x}, t) + r\int_0^t d\tau\, e^{-r\tau}\, \mathcal{G}_0(\vec{x}, \tau)\,. \tag{1.8}$$

The first term corresponds to the trajectories where no resetting has occurred up to time t, which happens with probability $\Psi(t) = \int_t^\infty \psi(\tau')\, d\tau' = 1 - \int_0^t \psi(\tau')\, d\tau' = e^{-rt}$; in this case, the JPDF is simply that of the process without resetting $\mathcal{G}_0(\vec{x}, t)$. The second term considers instead the trajectories where the last resetting has occurred at time $t-\tau$, and then the particles propagate freely in the subsequent interval $[t-\tau, t]$. In the above case, the probability of a reset at time $t-\tau$ and then no reset up to t is simply $r\, d\tau\, e^{-r\tau}$. The stationary state is obtained in the limit $t \to \infty$ and is given by

$$\mathcal{P}_r^*(\vec{x}) = r\int_0^\infty d\tau\, e^{-r\tau} \prod_{i=1}^N \frac{1}{\sqrt{4\pi D\tau}} \exp\left(-\frac{x_i^2}{4D\tau}\right)\,. \tag{1.9}$$

This expression can be interpreted as follows: the JPDF is constructed by evaluating the N-particles diffusive propagator at a time τ, and then averaging over the distribution $re^{-r\tau}$, which represents the probability that the last reset occurred at time $t-\tau$, with no further resets thereafter.

An important observation is that, after integrating over τ, Eq. (1.9) no longer factorizes into a product of single-particle distributions. This implies that the particles become correlated in the stationary state, despite being dynamically independent between resets.

This structure is a particular instance of a more general class introduced in [40], in which the variables are said to be *conditionally independent and identically distributed* (c.i.i.d.) variables. We illustrate this concept in Section 2.1.1.

Chapter 2

Non-Poissonian simultaneous stochastic resetting of N diffusing particles

2.1 Stationary state

We aim to generalize the system introduced above to the case where $\psi(\tau)$ is a general waiting time distribution, not necessarily exponential. In this scenario, we can no longer treat each infinitesimal time interval dt as independent, as in the Poissonian case. Nevertheless, it is still possible to derive an expression for the NESS.

To clarify the process, let us describe how it is simulated: after each reset, we sample a time τ^* from the distribution $\psi(\tau)$ and simulate N independent diffusive particles for a duration τ^*. The position of each particle evolves according to the update rule:

$$x_i(t + \Delta t) = x_i(t) + \sqrt{2D\Delta t}\,\eta_i(t).$$

The subscript i, with $i = 1, ..., N$, labels the particles and $\{\eta_i(t)\}_{i=1...,N}$ are independent Gaussian white noises satisfying $\langle \eta_i(t)\eta_j(t')\rangle = \delta_{ij}\delta(t - t')$. Once the time τ^* has elapsed, all particles are simultaneously reset to the origin, a new value of τ^* is sampled from $\psi(\tau)$, and the process repeats.

The steady-state behavior of a *single particle* subject to non-Poissonian resetting has been investigated using several different approaches, as summarized in [36]. In particular, the case of power-law resetting times is studied in [37], while the effect of a time-dependent resetting rate $r(t)$ is discussed in [15]. More generally, [38] introduces a generalized master equation that captures arbitrary waiting time distributions between resets.

In this work, we provide a derivation that is particularly suited to our scenario, based on the last renewal approach introduced earlier. This method classifies all trajectories contributing to the JPDF $\mathcal{P}(\vec{x}, t)$ into two categories:

1. Trajectories that have not experienced any reset up to time t;

2. Trajectories that have experienced at least one reset before time t.

These two types of trajectories are illustrated in Figure 2.1. To compute their contribution to the total JPDF, we introduce the function $\Psi(t) = \int_t^\infty \psi(\tau')\,d\tau'$, which gives the probability that no reset has occurred up to time t. For trajectories of the first type, the system evolves via

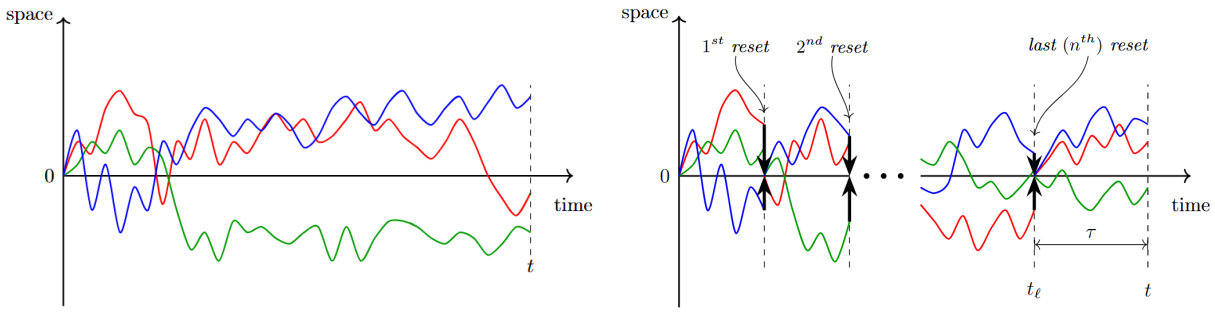

Figure 2.1: **Schematic illustration of the process.** The left panel shows the sketch of a trajectory where no reset occurs up to time t: the particles evolve purely by free diffusion. The right panel shows the sketch of a trajectory that undergoes at least one reset before time t. The last reset occurs at time t_ℓ, and there are $n-1$ resets before it, with $n \geq 1$. We explicitly show the first, the second, and the last (n^{th}) reset.
Since each reset completely deletes the system's past, the state of the system at time t depends only on the time interval $\tau = t - t_\ell$ since the last reset. The statistical properties of this time interval τ are effectively described, in the stationary state, by the function $h(\tau)$ defined in 2.7.

free diffusion over the interval $[0, t]$, contributing with $\Psi(t)\, \mathcal{G}_0(\vec{x}, t)$ to the JPDF, where $\mathcal{G}_0$ is the free propagator defined in Eq. (1.7).

We now consider trajectories that have experienced at least one reset before time t. Due to the renewal nature of the process, the system's statistical properties at time t depend only on the time since the *last* reset, not on the entire history. Let $t_\ell \in [0, t]$ denote the time of the last reset. The key object is $\Upsilon(t_\ell)$, the total probability density that the last reset occurred exactly at time t_ℓ, regardless of how many previous resets happened before.

This function can be written as:

$$\Upsilon(t_\ell) = \sum_{n=1}^{\infty} \upsilon_n(t_\ell), \tag{2.1}$$

where $\upsilon_n(t_\ell)$ is the probability density that exactly the n^{th} reset occurs at time t_ℓ. Since any number of resets can happen before the last one, we sum over all $n \geq 1$.

The contribution to the JPDF from such trajectories is:

$$\int_0^t dt_\ell\, \Upsilon(t_\ell)\, \Psi(t - t_\ell)\, \mathcal{G}_0(\vec{x}, t - t_\ell). \tag{2.2}$$

In other words, the last reset occurs at time t_ℓ with probability $\Upsilon(t_\ell)\, dt_\ell$. From that point until time t, no further reset occurs, which happens with probability $\Psi(t - t_\ell)$. During this interval, the particles evolve freely according to the propagator $\mathcal{G}_0(\vec{x}, t - t_\ell)$. Since t_ℓ can take any value in $(0, t)$, we integrate over it.

We thus obtain the last renewal equation for a general resetting protocol $\psi(\tau)$:

$$\mathcal{P}(\vec{x}, t) = \Psi(t)\, \mathcal{G}_0(\vec{x}, t) + \int_0^t dt_\ell\, \Upsilon(t_\ell)\, \Psi(t - t_\ell)\, \mathcal{G}_0(\vec{x}, t - t_\ell). \tag{2.3}$$

To evaluate $\Upsilon(t)$, we notice that the functions $\upsilon_n(t)$ satisfy the recursion:

$$\upsilon_n(t) = \int_0^t d\tau\, \psi(t-\tau)\, \upsilon_{n-1}(\tau), \quad \text{with} \quad \upsilon_1(t) = \psi(t).$$

Taking the Laplace transform (denoted by a tilde), we find $\tilde{\upsilon}_n(s) = [\tilde{\psi}(s)]^n$. Summing over all $n \geq 1$, we obtain:

$$\tilde{\Upsilon}(s) = \sum_{n=1}^{\infty} [\tilde{\psi}(s)]^n = \frac{\tilde{\psi}(s)}{1-\tilde{\psi}(s)}.$$

We now take the Laplace transform of equation (2.3). Substituting the expression for $\tilde{\Upsilon}(s)$, we get:

$$\tilde{\mathcal{P}}(\vec{x}, s) = \frac{1}{1-\tilde{\psi}(s)} \int_0^{\infty} dt\, e^{-st}\, \Psi(t)\, \mathcal{G}_0(\vec{x}, t). \tag{2.4}$$

Recalling that $\psi(t) = -\frac{d\Psi(t)}{dt}$, the Laplace transform of $\Psi(t)$ is given by:

$$\tilde{\Psi}(s) = \frac{1-\tilde{\psi}(s)}{s}.$$

Inserting this into equation (2.4) leads to the final expression:

$$\tilde{\mathcal{P}}(\vec{x}, s) = \frac{1}{s\,\tilde{\Psi}(s)} \int_0^{\infty} dt\, e^{-st}\, \Psi(t)\, \mathcal{G}_0(\vec{x}, t). \tag{2.5}$$

A stationary state exists in the limit $t \to \infty$ provided that $\psi(t)$ decays sufficiently fast. In this limit, the stationary state is obtained from the coefficient of $1/s$ in the Laplace domain (as $s \to 0$), leading to

$$\mathcal{P}^*(\vec{x}) = \mathcal{P}^*(\vec{x}, t \to \infty) = \frac{\int_0^{\infty} dt\, \Psi(t)\, \mathcal{G}_0(\vec{x}, t)}{\int_0^{\infty} dt\, \Psi(t)}\,. \tag{2.6}$$

provided that this limit exists. A sufficient condition is that $\int_0^{\infty} dt\, \Psi(t) < \infty$, which implies that $\psi(t)$ should decay to zero faster than $1/t^2$. If it is not the case, the system does not reach any stationary state. Since the resetting move breaks detailed balance, when a stationary state exists, it is as a non-equilibrium one.
It is now convenient to define a normalized weight function

$$h(\tau) = \frac{\Psi(\tau)}{\int_0^{\infty} dt\, \Psi(t)}\,, \tag{2.7}$$

so that the stationary state can be written as

$$\mathcal{P}^*(\vec{x}) = \int_0^{\infty} d\tau\, h(\tau)\, \mathcal{G}_0(\vec{x}, \tau) = \int_0^{\infty} d\tau\, h(\tau) \prod_{i=1}^{N} \frac{1}{\sqrt{4\pi D\tau}} \exp\left(-\frac{x_i^2}{4D\tau}\right)\,. \tag{2.8}$$

This expression makes the c.i.i.d. nature [40] of the problem explicit.
To understand the meaning of the distribution $h(\tau)$ we notice that, integrating by parts, we can write $\int_0^{\infty} d\tau\, \Psi(\tau) = \langle \tau \rangle$. Thus, the normalization constant is $\langle \tau \rangle$, i.e. the average waiting time between resets. In the stationary state, time-translation invariance implies that the probability of a reset occurring at any time is constant and equal to $\frac{1}{\langle \tau \rangle}$.

We can then interpret the quantity

$$h(\tau)\,d\tau = \frac{1}{\langle\tau\rangle}\,\Psi(\tau)\,d\tau$$

as the joint probability of two independent events: first, that the last reset happened in the time interval $[t-\tau, t-\tau+d\tau]$, which occurs with probability $\frac{1}{\langle\tau\rangle}\,d\tau$; and second, that no further resets occurred in the interval $[t-\tau, t]$, which happens with probability $\Psi(\tau)$. This interpretation reflects the fact that the state of the system depends only on the time elapsed since the last reset, and not on the full history before it (see Figure 2.1).

The quantity $\frac{1}{\langle\tau\rangle}$ is an effective rate of resetting in the stationary state, which is proportional to the rate r, but they are equal only for an exponential time distribution. In fact, when $\psi(\tau) = re^{-r\tau}$, the probability $\Psi(\tau) = e^{-r\tau}$ and we get $\psi(\tau) = h(\tau)$. This implies that the stationary state will be given by (1.9). To compare different distributions, we introduce a rate r, whose inverse defines the resetting time scale and we define the dimensionless function $\tilde{h}(z)$ as:

$$h(\tau) = r\tilde{h}(r\tau) \tag{2.9}$$

2.1.1 Observables and c.i.i.d. structure

As anticipated in the introduction, the system we are studying has a particular structure for which the variables are said to be c.i.i.d. This particular structure is what allows us to calculate many observables of interest, even in the presence of strong correlations. In general, if we take N random variables (RV) $x_1, ..., x_N$, they are said to be conditionally independet and identically distributed (c.i.i.d.) if their JPDF can be written in the form

$$\text{Prob}\{x_1, \ldots, x_N\} = \int \left(\prod_{i=1}^{N} \text{Prob}\{x_i \mid \vec{Y}\} \right) \text{Prob}\{\vec{Y}\}\,d\vec{Y}\,. \tag{2.10}$$

meaning that the variables x_i are i.i.d. variables sampled from a probability distribution $\text{Prob}\{x_i \mid \vec{Y}\}$, where $\vec{Y} = \{y_1, ..., y_M\}$ is a set of random parameters with JPDF $\text{Prob}\{\vec{Y}\}$. If we fix the value of the parameters $\vec{Y}$, the variables x_i are independently drawn, but once we average on $\text{Prob}\{\vec{Y}\}$ they get correlated. In our specific case, the only random parameter is the time τ passed after the last reset.

Regardless of the form of the distribution $\psi(\tau)$ and hence of $h(\tau)$, the stationary state distribution in Eq. (2.8) exhibits an explicit c.i.i.d. structure. Thanks to this structure, a wide variety of observables O of the system can be computed as:

$$O = \int_0^\infty d\tau\, h(\tau) O(\tau) \tag{2.11}$$

where $O(\tau)$ is the observable O calculated for a fixed value of the parameter τ.

We begin by considering the average particle density in the stationary state, which is defined as:

$$\rho_N(x) = \frac{1}{N}\left\langle \sum_{i=1}^{N} \delta(x - x_i) \right\rangle .$$

where $\langle ... \rangle$ indicates the average over $\mathcal{P}^*(\vec{x})$. Due to the symmetry between particles, $\rho_N(x)$

coincides with the one-point marginal of the stationary distribution:

$$\rho_N(x) = \mathcal{P}_{\text{stat}}(x) = \int_{-\infty}^{\infty} dx_1 \cdots \int_{-\infty}^{\infty} dx_{N-1}\, \mathcal{P}^*(\vec{x}) = \int_0^{\infty} d\tau\, h(\tau)\, p_0(x \mid \tau)\,. \tag{2.12}$$

where $p_0(x \mid \tau) = \frac{1}{\sqrt{4\pi D\tau}} \exp\left(-\frac{x^2}{4D\tau}\right)$ is the free propagator for a single particle. It is important to emphasize that this does not imply the particles are uncorrelated, as Eq. (2.6) does not factorise.

Although the particles are correlated, the symmetry of the system ensures that the first-order connected correlator $\langle x_i x_j \rangle_c = \langle x_i x_j \rangle - \langle x_i \rangle \langle x_j \rangle$ vanishes. Instead, one can study the second-order connected correlations such as $\langle x_i^2 x_j^2 \rangle_c = \langle x_i^2 x_j^2 \rangle - \langle x_i^2 \rangle \langle x_j^2 \rangle$. It is easy to show that

$$\langle x_i^2 x_j^2 \rangle_c = \int_0^{\infty} d\tau\, h(\tau)\, \left(\sigma^2(\tau)\right)^2 - \left(\int_0^{\infty} d\tau\, h(\tau)\, \sigma^2(\tau)\right)^2 \tag{2.13}$$

where $\sigma^2(\tau) = 2D\tau$ is the variance of the gaussian propagator. Eq. (2.13) can be seen as the variance of the quantity $\sigma^2(\tau)$ with respect to the distribution $h(\tau)$.
To explore local observables, it is convenient to order particle positions in decreasing order and relabel them as $\{M_1 = \max_{i=1,\dots,N} x_i > M_2 > \cdots > M_N = \min_{i=1,\dots,N} x_i\}$. This allows us to study quantities such as the probability $\text{Prob}\{M_k = \omega\}$ that the k^{th} largest particle is at position ω, or the probability $\text{Prob}\{d_k = g\}$ that the distance $d_k = M_k - M_{k+1}$ between consecutive particles is equal to g in the stationary state. Thanks to the c.i.i.d. structure, as noted above, we can write:

$$\text{Prob}\{M_k = \omega\} = \int_0^{\infty} d\tau\, h(\tau) \text{Prob}\{M_k(\tau) = \omega\} \tag{2.14}$$

where $M_k(\tau)$ is the maximum of N independent variables sampled from a Gaussian with zero mean and variance $2D\tau$. This is equivalent to saying that $M_k(\tau)$ is the k^{th} maximum between the particles' positions given that a time τ has elapsed since the last reset. In the large N limit, as shown in [40], this distribution converges to

$$\text{Prob}\{M_k = w\} \xrightarrow{N\to\infty} \int \mathrm{d}\tau\, h(\tau)\, \delta\left(w - q(\alpha, \tau)\right) \tag{2.15}$$

having defined $k = \alpha N$ with $0 < \alpha < 1$. By setting $\alpha = O(1)$, we access the regime of the order statistics, whereas choosing $\alpha = O\left(\frac{1}{N}\right)$ leads to the study of the EVS. The value $q(\alpha, \tau)$ corresponds to the α-quantile of the conditional distribution $p_0(x \mid \tau)$:

$$\int_{q(\alpha,\tau)}^{+\infty} p_0(x \mid \tau)\, \mathrm{d}x = \alpha. \tag{2.16}$$

It is the value of x such that there are, on average, αN variables above $q(\alpha, \tau)$. In our specific case $p_0(x \mid \tau) = \frac{1}{\sqrt{4\pi D\tau}} \exp\left(-\frac{x_i^2}{4D\tau}\right)$ and $q(\alpha, \tau)$ takes the explicit form $q(\alpha, \tau) = \sqrt{4D\tau}\, \text{erfc}^{-1}(2\alpha)$.

Also for the spacing between particles, we can write

$$\text{Prob}\{d_k = g\} = \int_0^{\infty} d\tau\, h(\tau)\, \text{Prob}\{d_k(\tau) = g\}. \tag{2.17}$$

where $d_k(\tau) = M_k(\tau) - M_{k+1}(\tau)$ is the distance between two consecutive particles given that a time τ is passed since the last reset. In the limit $N \to \infty$ eq. (2.17) becomes

$$\text{Prob}\{d_k = g\} = \int_0^\infty d\tau\, h(\tau)\, Np(q,\tau) e^{-Np(q,\tau)g} \tag{2.18}$$

where $q = q(\alpha,\tau) = \sqrt{4D\tau}\text{erfc}^{-1}(2\alpha)$, $k = \alpha N$, and $p(q,\tau) = \frac{1}{\sqrt{4\pi D\tau}} \exp\left([-\text{erfc}^{-1}(2\alpha)]^2\right)$.

Another observable of interest is the full counting statistics (FCS), i.e., the probability $P(N_L, N)$ of finding N_L particles out of N within a symmetric interval $[-L, L]$ centered around the resetting point $x = 0$. To compute it for our gas we can use the c.i.i.d. structure of our system and write:

$$P(N_L, N) = \int_0^\infty d\tau\, h(\tau) \binom{N}{N_L} [\tilde{q}(\tau)]^{N_L} [1 - \tilde{q}(\tau)]^{N - N_L}. \tag{2.19}$$

where $\tilde{q}(\tau) = \int_{-L}^{L} p(y,\tau)\, dy = \text{erf}\left(\frac{L}{\sqrt{4D\tau}}\right)$ is the probability of a brownian particle diffusing for a time τ to be inside the interval $[-L, L]$. The function inside the integral (2.19) that multiplies $h(\tau)$ is just a binomial distribution that accounts for having N_L out of the total N particles inside the box. As N increases, the binomial distribution inside the integral (2.19) becomes sharply peaked around $\tilde{q}(\tau)$ and the equation simplifies to:

$$P(N_L, N) \approx \int_0^\infty d\tau\, h(\tau) \delta(\kappa - \tilde{q}(\tau)). \tag{2.20}$$

where $k = \frac{N_L}{N}$.

In the following sections, we study these observables in detail and we find that all of them admit a scaling form with a scaling function explicitly governed by the function $h(\tau)$. Moreover, certain universal features emerge: for example, all observables have their own scale factor, meaning a characteristic scale that sets their overall magnitude, which is universal, i.e. it is independent of the specific resetting protocol. Notably, the behaviors for small values of the arguments of $\rho_N(x)$, $\text{Prob}\{M_k = \omega\}$, and $\text{Prob}\{d_k = g\}$ are independent of the form of $h(\tau)$. A similar universal behavior appears in the FCS when taking the limit $N_L \to N$. Conversely, in the large-x, large-ω, large-g or small-N_L regime, the observables depend only on the large-τ tail of $h(\tau)$, and we have derived explicit results for three general classes of tail behaviors. Since the observables M_k and d_k have been widely studied in the literature for i.i.d. variables [44–47], we compare some of these classical results to our case in order to see how correlations change these observables in this case. We illustrate three concrete cases for $\psi(\tau)$ in section 2.2 before giving the general results in section 2.3.

2.2 Analytical results for three particular resetting protocols

We now study the behaviour of the system for three specific examples of the resetting time distribution $\psi(\tau)$. This will provide concrete insight before generalizing the results to an arbitrary $h(\tau)$ in Section 2.3. We begin with the well-studied Poissonian case, for which $\psi(\tau) = re^{-r\tau}$, and then examine two qualitatively different situations: a distribution with a power-law tail and

one with a bounded support. These two cases were chosen because they exhibit significantly different behaviors at large τ, leading to distinct outcomes for all the observables of interest.

Poissonian resetting protocol

We begin with the Poissonian resetting case introduced in Sec. 1.2, corresponding to the inter-reset time distribution $\psi(\tau) = re^{-r\tau}$. Physically, this distribution arises because, in each small interval dt, the particles reset with probability $r\,dt$ and they diffuse otherwise.

In this context, $h(\tau)$ coincides with the inter-reset distribution $\psi(\tau)$. This equivalence can be shown by noting that:

$$h(\tau)d\tau = \frac{\Psi(\tau)}{\langle\tau\rangle}d\tau = \langle r\rangle\Psi(\tau)d\tau,$$

where $\langle r\rangle = 1/\langle\tau\rangle$ is the average resetting rate, and $\Psi(\tau)$ is the probability of no resets occurring within the interval $[t-\tau, t]$. For the exponential distribution specifically, we have:

$$\langle r\rangle = r \quad \text{and} \quad \Psi(\tau) = e^{-r\tau},$$

implying directly $h(\tau) = \psi(\tau) = re^{-r\tau}$. Knowing $h(\tau)$, one can employ Eq. (2.12) to obtain the steady-state density:

$$\rho_N(x) = \frac{1}{2}\sqrt{\frac{r}{D}}\,\exp\left(-\sqrt{\frac{r}{D}}\,|x|\right). \tag{2.21}$$

Thus, the density decays exponentially with the characteristic length scale $l = \sqrt{\frac{D}{r}}$. This prediction has been experimentally verified using colloidal particles as the diffusing agents and optical tweezers to implement the resetting mechanism [30].

Although the particles diffuse independently between resets, the resetting mechanism introduces strong correlations. This is evident from the fact that the JPDF (2.8) does not factorise. By symmetry, the first non-zero correlator is given by

$$\langle x_i^2 x_j^2\rangle_c = \frac{4D^2}{r^2} \quad \forall\, i, j\,. \tag{2.22}$$

which indicates strong correlations at all distances. It is important to note that these correlations arise purely from the dynamics of the system, as the particles do not interact directly. The order and extreme value statistics are addressed next by studying the k-th maximum, M_k, among the particle positions. Substituting $h(\tau) = r\,e^{-r\tau}$ into Eq. (2.15) and evaluating the integral yields

$$\text{Prob}\{M_k = \omega\} = \frac{1}{\Lambda(\alpha)}\,S\left(\frac{\omega}{\Lambda(\alpha)}\right), \tag{2.23}$$

with the scaling function

$$S(z) = 2ze^{-z^2}, \tag{2.24}$$

and the scaling factor

$$\Lambda(\alpha) = \sqrt{\frac{4D}{r}}\,\text{erfc}^{-1}(2\alpha) \quad \text{with} \quad \alpha = \frac{k}{N}. \tag{2.25}$$

The parameter $\Lambda(\alpha)$ sets the typical scale of values taken by M_k. By varying α, we can

probe either the bulk or edge behavior of the gas: for $\alpha = O(1)$, we sample the bulk, where $\Lambda(\alpha) \sim O(1)$; for $\alpha = O(1/N)$, we probe the edges, where $\Lambda(\alpha)$ converges to $L_N = \sqrt{\frac{4D \ln N}{r}}$. Despite this change in scale, the scaling function $S(z)$ remains unchanged, and it remains valid both for the order and the extreme value statistics. As a result, while the density $\rho_N(x)$ spans the full line, the rightmost particle is typically located at a distance $O(\sqrt{\ln N})$ from the origin.

Furthermore, the distance d_k between consecutive particles is given by

$$\text{Prob}\{d_k = g\} = \frac{1}{\lambda_N(\alpha)} D\left(\frac{g}{\lambda_N(\alpha)}\right) , \tag{2.26}$$

where

$$D(z) = 2\int_0^\infty du\, \exp\left(-u^2 - \frac{z}{u}\right) , \tag{2.27}$$

and the scaling factor is

$$\lambda_N(\alpha) = \frac{1}{Nb\sqrt{r}} \quad \text{with} \quad b = \frac{\exp\left(-\left[\text{erfc}^{-1}(2\alpha)\right]^2\right)}{\sqrt{4\pi D}} . \tag{2.28}$$

This result holds both in the bulk and near the edges. It is worth noting that $\lambda_N(\alpha)$ is $O(1/N)$ in the bulk, while at the edges it behaves as $\lambda_N(\alpha) \to l_N = \sqrt{\frac{D}{rk^2 \ln N}}$, indicating an inhomogeneous gas: particles are very closely packed in the bulk and much sparser at the boundaries. The scaling function $D(z)$ behaves as

$$D(z) \approx \begin{cases} \sqrt{\pi} + 2z \ln z & z \to 0 \\ 2\sqrt{\frac{\pi}{3}} \exp\left(-3\left(\frac{z}{2}\right)^{2/3}\right) & z \to \infty \end{cases} \tag{2.29}$$

Finally, the full counting statistics (FCS) are derived from Eq. (2.20):

$$H(\kappa) = \gamma\sqrt{\pi}\,[u(\kappa)]^{-3} \exp\left(-\frac{\gamma}{[u(\kappa)]^2} + [u(\kappa)]^2\right) , \tag{2.30}$$

where $k = \frac{N_L}{N}$ represents the fraction of particles inside the box $[-L, L]$. The asymptotics are

$$H(\kappa) \sim \begin{cases} \frac{8\gamma}{\pi\kappa^3} \exp\left(-\frac{4\gamma}{\pi\kappa^2}\right) , & \kappa \to 0 \\ \frac{\gamma\sqrt{\pi}}{(1-\kappa)^{3/2}\,[\ln(1-\kappa)]^{3/2}} , & \kappa \to 1 , \end{cases} \tag{2.31}$$

implying that $H(\kappa)$ vanishes rapidly as $\kappa \to 0$ and diverges in an integrable way as $\kappa \to 1^-$. All these theoretical predictions have been confirmed numerically in [39].

Power-law resetting protocol

Next, we examine a power-law distribution for the resetting times:

$$\psi(\tau) = \frac{r\beta}{(r\tau)^{1+\beta}} , \tag{2.32}$$

defined for $\tau \in [1/r, \infty)$ and for $\beta > 0$. To ensure a stationary state (i.e. finite $\langle \tau \rangle$), we restrict the discussion to $\beta > 1$.

Using the definition (2.7) we first compute the normalization:

$$\int_0^\infty dt\, \Psi(t) = \frac{\beta}{\beta - 1} \frac{1}{r}\,,$$

which leads to

$$h(\tau) = \begin{cases} \dfrac{\beta - 1}{\beta}\, r, & \tau < 1/r\,, \\ \dfrac{\beta - 1}{\beta}\, r\, (r\tau)^{-\beta}, & \tau > 1/r\,. \end{cases} \tag{2.33}$$

Inserting eq. (2.33) in eq. (2.12) we can write the density $\rho_N(x)$ in the scaling form

$$\rho_N(x) = \frac{1}{l}\, R\Big(\frac{x}{l}\Big)\,, \tag{2.34}$$

where the scaling parameter $l = \sqrt{\frac{D}{r}}$ is the same as in the Poissonian case and where the scaling function $R(z)$ is given by

$$R(z) = \frac{z}{4\sqrt{\pi}} \frac{\beta - 1}{\beta} \left\{ \Gamma\left(-\frac{1}{2}, \frac{z^2}{4}\right) + \left(\frac{2}{z}\right)^{2\beta} \gamma\left(\beta - \frac{1}{2}, \frac{z^2}{4}\right) \right\}. \tag{2.35}$$

The functions $\Gamma(s, z)$ and $\gamma(s, z)$ are respectively the upper and lower incomplete gamma functions, defined as $\Gamma(s, z) = \int_0^z dy\, y^{s-1}\, e^{-y}$ and $\gamma(s, z) = \int_z^\infty dy\, y^{s-1}\, e^{-y}$. The resulting density profile, shown in Figure 2.2, exhibits the following asymptotic behaviors:

$$R(z) \approx \begin{cases} A_1 - A_2\, |z|, & z \to 0\,, \\ \dfrac{A_3}{z^{2\beta - 1}}, & z \to \infty\,. \end{cases} \tag{2.36}$$

where A_1, A_2 and A_3 are positive constants. This result is particularly interesting because it tells us that the power-law resetting distribution leads to a power-law tail in the particle density, in contrast with the exponential decay found in the Poissonian case. Although the scale factor l remains unchanged, longer diffusion intervals occur with a higher probability, allowing particles to move further from the origin. This results in a fat-tail density.

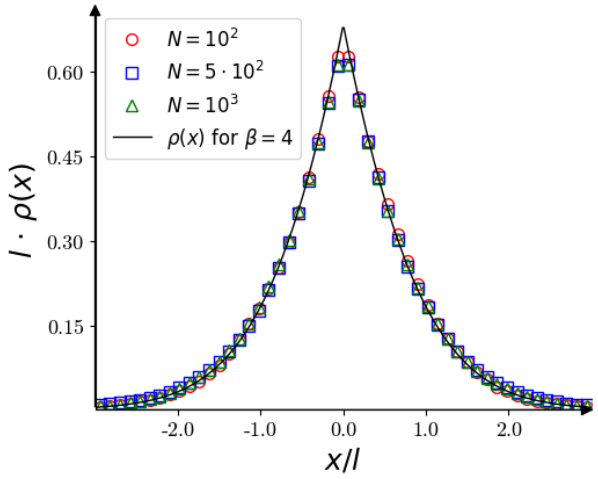

Figure 2.2: Plot of the density profile $\rho_N(x) = \frac{1}{l} R\left(\frac{x}{l}\right)$. The scaling function $R(z)$ is given in (2.35), and $l = \sqrt{\frac{D}{r}}$. The solid black curve shows the theoretical prediction for the resetting protocol $\psi(t) = \frac{r\beta}{(rt)^{1+\beta}}$ with $t \in [1/r, \infty)$ and $\beta = 4$. The symbols indicate simulation results for different values of N. Simulations were performed with $r = 1$ and $D = \frac{1}{2}$.

In the NESS, correlations are again strong. The first non-zero correlator is

$$\langle x_i^2 x_j^2 \rangle_c = \langle x_i^2 x_j^2 \rangle - \langle x_i^2 \rangle \langle x_j^2 \rangle = \frac{4D^2}{r^2} \frac{(\beta-1)(\beta^2-4\beta+7)}{12(\beta-3)(\beta-2)^2} \quad \forall\, i, j\,, \tag{2.37}$$

which is defined for $\beta > 3$,i.e. when the resetting time variance is finite.

The order and extreme value statistics are modified as well. One finds

$$\text{Prob}\{M_k = \omega\} = \frac{1}{\Lambda(\alpha)} S\left(\frac{\omega}{\Lambda(\alpha)}\right)\,, \tag{2.38}$$

with the scaling function $S(z)$, whose shape is shown in Figure 2.3, given by

$$S(z) = \begin{cases} 2\frac{\beta-1}{\beta}\, z, & z < 1\,, \\ 2\frac{\beta-1}{\beta}\, \frac{1}{z^{2\beta-1}}, & z > 1\,. \end{cases} \tag{2.39}$$

The scaling factor $\Lambda(\alpha)$ remains the same as in the Poissonian case.

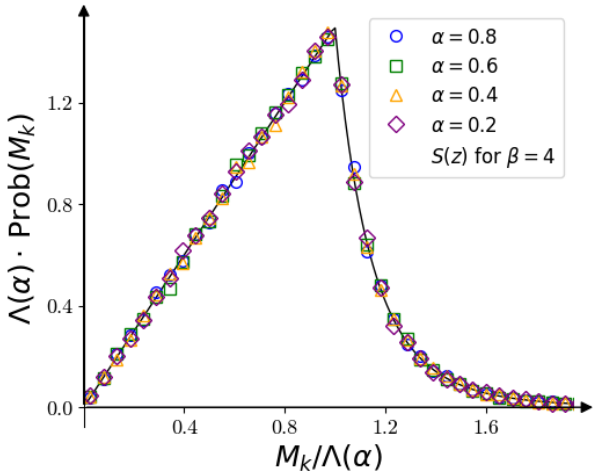

Figure 2.3: Plot of the distribution of the k^{th} rightmost particle M_k. The distribution follows the scaling form $\text{Prob}\{M_k = \omega\} = \frac{1}{\Lambda(\alpha)} S\left(\frac{\omega}{\Lambda(\alpha)}\right)$, where the scaling function $S(z)$ is given in (2.39), and the scaling parameter $\Lambda(\alpha)$ is defined in (2.25). The solid black curve represents the theoretical prediction for the resetting protocol $\psi(t) = \frac{r\beta}{(rt)^{1+\beta}}$ with $t \in [1/r, \infty)$ and $\beta = 4$. Different symbols correspond to different values of $\alpha = \frac{k}{N}$. Simulations were performed with $N = 10^6$ particles, using $r = 1$ and $D = \frac{1}{2}$.

The density $\rho_N(x)$ is also the one-point marginal of the particles' positions, and one may compare the above EVS, given by (2.38) for $k = O(1)$, with that obtained by sampling N i.i.d. random variables from $\rho_N(x)$. In this latter case, the limit $N \to \infty$ gives a Fréchet distribution $\tilde{S}(z) = \frac{\alpha}{z^{\alpha+1}} e^{-z^{-\alpha}}$ with parameter $\alpha = 2\beta - 2$ (see appendix A.1). It behaves as

$$\tilde{S}(z) \approx \begin{cases} \exp\left[-z^{-(2\beta-2)}\right], & z \to 0\,, \\ \dfrac{1}{z^{2\beta-1}}, & z \to \infty\,. \end{cases} \tag{2.40}$$

Thus, the resetting protocol increases the probability mass near the origin while preserving the power-law tail for large z.

The scaling function for the spacing distribution is obtained from Eq. (2.18):

$$D(z) = 2\frac{\beta-1}{\beta}\left[e^{-z} - z\,\Gamma(0,z) + z^{2\beta-1}\left\{\Gamma(2\beta-1) - \gamma\left(2\beta-1, z\right)\right\}\right], \tag{2.41}$$

and its shape is shown in Figure 2.4. The function $\Gamma(z) = \int_0^\infty dy\, y^{z-1}\, e^{-y}$ is the gamma function, while $\Gamma(s,z)$ and $\gamma(s,z)$ are the upper and lower incomplete gamma functions defined above.

It follows that the probability for the k-th spacing is

$$\text{Prob}\{d_k = g\} = \frac{1}{\lambda_N(\alpha)} D\left(\frac{g}{\lambda_N(\alpha)}\right). \tag{2.42}$$

The asymptotic behaviors of $D(z)$ are

$$D(z) \approx \begin{cases} A_4 + A_5 z \ln z, & z \to 0\,, \\ \dfrac{A_6}{z^{2\beta-1}}, & z \to \infty\,. \end{cases} \tag{2.43}$$

where A_4, A_5 and A_6 are positive constants. As for the distribution of the maximum, we find that the scale $\lambda_N(\alpha)$ is unchanged, and the $z \to 0$ behavior remains the same as in the Poissonian case. However, for large z, the distribution exhibits a power-law tail instead of a stretched exponential. This means that a power-law resetting protocol, by allowing longer diffusing intervals, also leads to a sparser particle gas.

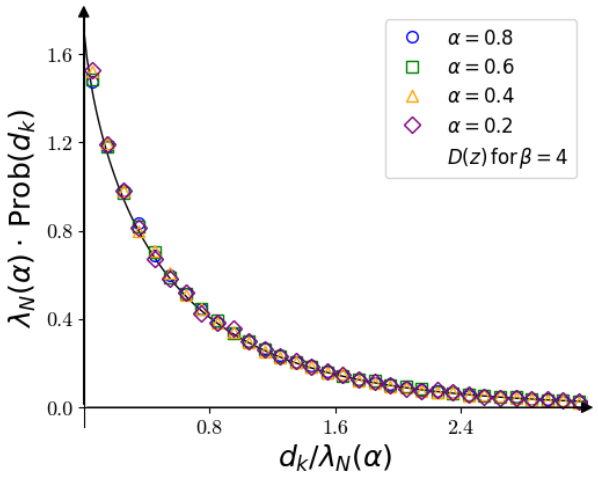

Figure 2.4: Plot of the distribution of the spacing $d_k = M_k - M_{k-1}$ between the k^{th} and $(k-1)^{th}$ rightmost particles. The distribution follows the scaling form $\text{Prob}\{d_k = g\} = \frac{1}{\lambda_N(\alpha)} D\left(\frac{g}{\lambda_N(\alpha)}\right)$, where the scaling function $D(z)$ is given by (2.41), and the scaling parameter $\lambda_N(\alpha)$ is defined in (2.28). The solid black curve represents the theoretical prediction for the resetting protocol $\psi(t) = \frac{r\beta}{(rt)^{1+\beta}}$ with $t \in [1/r, \infty)$ and $\beta = 4$. Different symbols correspond to different values of $\alpha = \frac{k}{N}$. The simulations were performed with $N = 10^6$ particles, using $r = 1$ and $D = \frac{1}{2}$.

It can also be interesting to compare this distribution with what we would have obtained sampling N i.i.d. random variables from the average density $\rho_N(x)$. For the Fréchet class, as in this case, the asymptotic scaling function $\tilde{D}(z)$ for the distribution of d_1 is such that (cf. Appendix A.1):

$$\tilde{D}(z) \approx \begin{cases} A_7 - A_8 z & z \to 0 \\ \frac{\alpha}{(k-1)!} \frac{1}{z^{1+\alpha}} & z \to \infty \end{cases} \tag{2.44}$$

where A_7 and A_8 are positive constants and $\alpha = 2\beta - 2$. Thus, we have a slightly different behavior for small z, but the tails at $z \to \infty$ of (2.43) and eq. (2.44) are the same.

The full counting statistics (FCS) are given by $P(N_L, N) = \frac{1}{N} H\left(\frac{N_L}{N}\right)$, where

$$H(k) = \begin{cases} \sigma\sqrt{\pi}\left(\frac{\beta-1}{\beta}\right) u(k)^{-3} e^{u(k)^2}, & k > \mathrm{erf}(\sqrt{\sigma}) \ , \\ \sqrt{\pi}\,\sigma^{1-\beta}\left(\frac{\beta-1}{\beta}\right) u(k)^{2\beta-3} e^{u(k)^2}, & k < \mathrm{erf}(\sqrt{\sigma}) \ , \end{cases} \tag{2.45}$$

with $k = \frac{N_L}{N}$, $u(k) = \mathrm{erf}^{-1}(k)$ and $\sigma = \frac{rL^2}{4D}$. As $k \to 1^-$, one finds

$$H(k) \approx \sigma\sqrt{\pi}\left(\frac{\beta-1}{\beta}\right) \frac{1}{(1-k)\,|\ln(1-k)|^{3/2}},$$

which diverges in an integrable manner (see Figure 2.5), exactly as in the Poissonian case. In contrast, as $k \to 0$, $H(k)$ behaves as

$$H(k) \approx \sqrt{\pi}\,\sigma^{1-\beta}\left(\frac{\beta-1}{\beta}\right)\left(\frac{\sqrt{\pi}}{2}\,k\right)^{2\beta-3} .$$

Thus, for $\beta > \frac{3}{2}$, the function decays to zero as a power law; it diverges in an integrable manner for $1 < \beta < \frac{3}{2}$, while for $\beta = \frac{3}{2}$, it remains constant. This behavior reflects the fact that a power-law tail resetting protocol, which allows for long intervals between resets, enables particles to travel far from the origin. As a result, small values of the particle fraction k become more likely compared to the Poissonian case in which $H(k)$ decays very fast as $k \to 0$ (2.31).

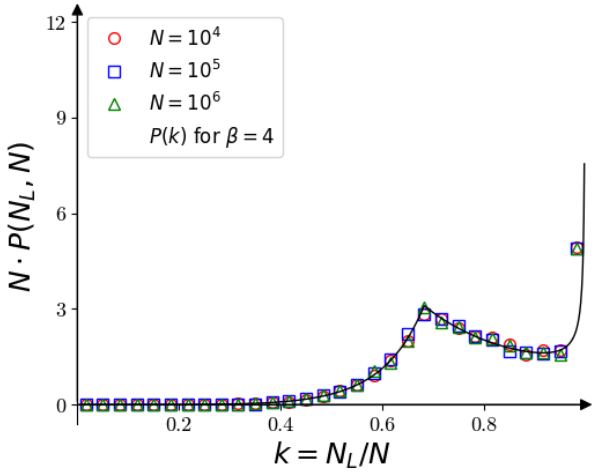

Figure 2.5: Plot of the full counting statistics given by the distribution $P(N_L, N) = \frac{1}{N} H\left(\frac{N_L}{N}\right)$. The scaling function $H(k)$ is given by (2.45). The solid black curve shows the theoretical prediction for the resetting protocol $\psi(t) = \frac{r\beta}{(rt)^{1+\beta}}$ with $t \in [1/r, \infty)$ and $\beta = 4$. The symbols indicate simulation results for different values of N. The simulations were done with $r = 1$ and $D = \frac{1}{2}$.

Bounded resetting protocol

Finally, we consider a resetting distribution with a finite support, defined as

$$\psi(\tau) = \frac{\gamma r}{T^\gamma}\,(T - r\tau)^{\gamma-1} \ , \tag{2.46}$$

for $\tau \in [0, T/r]$ and for any $\gamma > 0$. Since the distribution is bounded by $\tau = T/r$, the maximum time between resets is T/r. Using the definition

$$h(\tau) = \frac{\Psi(\tau)}{\int_0^\infty dt\, \Psi(t)}\,,$$

one finds

$$h(\tau) = \begin{cases} \dfrac{\gamma+1}{T^{\gamma+1}}\, r\, (T - r\tau)^\gamma\,, & \tau \in [0, T/r)\,, \\ 0, & \tau \geq T/r\,. \end{cases} \tag{2.47}$$

The average density of particles assumes again the scaling form

$$\rho_N(x) = \frac{1}{l}\, R\Big(\frac{x}{l}\Big)\,, \tag{2.48}$$

with

$$R(z) = \frac{\gamma+1}{T^{\gamma+1}\sqrt{\pi}} \int_0^{\sqrt{T}} du\, \left(T - u^2\right)^\gamma \exp\left[-\left(\frac{z}{2}\right)^2 \frac{1}{u^2}\right]\,, \tag{2.49}$$

and with the same scaling parameter $l = \sqrt{\frac{D}{r}}$ of the previous cases. The scaling function $R(z)$ behaves as

$$R\,(z) \approx \begin{cases} B_1 - B_2\,|z|, & z \to 0\,, \\ B_3 \exp\Big(-\frac{z^2}{T}\Big)\,, & z \to \infty\,. \end{cases} \tag{2.50}$$

and its shape, compared with simulation results, is shown in Fig. 2.6. The symbols B_1, B_2 and B_3 denote positive constants. The faster decay at large distances, compared to the Poissonian case, is a direct consequence of the finite cut-off in the resetting time distribution.

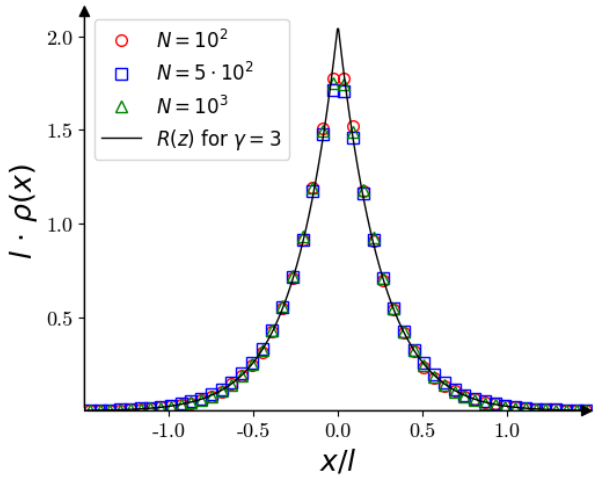

Figure 2.6: Plot of the density profile $\rho_N(x) = \frac{1}{l}\, R\left(\frac{x}{l}\right)$. The scaling function $R(z)$ is given in (2.49), and $l = \sqrt{\frac{D}{r}}$. The solid black curve shows the theoretical prediction for the resetting protocol $\psi(\tau) = \frac{\gamma r}{T^\gamma}\,(T - r\tau)^{\gamma-1}$ with $\tau \in [0, T/r]$, $\gamma = 3$, and $T = 1$. The symbols indicate simulation results for different values of N. Simulations were performed with $r = 1$ and $D = \frac{1}{2}$.

As in previous cases, the resetting mechanism generates strong correlations between particles.

Specifically, the second-order connected two-point correlator is given by

$$\langle x_i^2 x_j^2 \rangle_c = \langle x_i^2 x_j^2 \rangle - \langle x_i^2 \rangle \langle x_j^2 \rangle = \frac{4D^2}{r^2} \frac{\gamma+1}{(\gamma+2)^2(\gamma+3)} \quad \forall, i, j, , \tag{2.51}$$

which is smaller than that in Eq. (2.22) for any γ, but still indicates strong correlations.

Having characterized the correlations, we now turn to the order statistics of the system by studying the k^{th} maximum M_k among the particles' positions. Similarly to the Poissonian and power-law cases we can write

$$\text{Prob}\{M_k = \omega\} = \frac{1}{\Lambda(\alpha)} S\left(\frac{\omega}{\Lambda(\alpha)}\right) , \tag{2.52}$$

where, this time, the scaling function $S(z)$ is given by

$$S(z) = \begin{cases} \dfrac{2(\gamma+1)}{T^{\gamma+1}} z\,(T - z^2)^{\gamma}, & z < \sqrt{T}\,, \\ 0, & z \geq \sqrt{T}\,. \end{cases} \tag{2.53}$$

Here the typical distance scale $\Lambda(\alpha)$ is the same as in the earlier examples, both in the bulk and at the edges. This function, along with numerical data for various values of $\alpha = \frac{k}{N}$, is shown in Fig. 2.7.

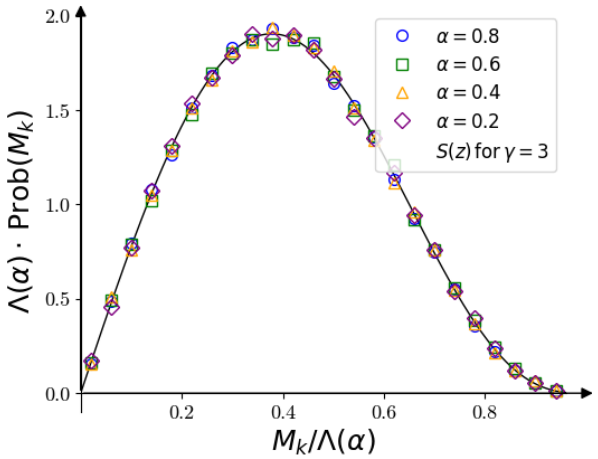

Figure 2.7: Plot of the distribution of the k^{th} rightmost particle M_k. The distribution follows the scaling form $\text{Prob}\{M_k = \omega\} = \frac{1}{\Lambda(\alpha)} S\left(\frac{\omega}{\Lambda(\alpha)}\right)$, where the scaling function $S(z)$ is given in (2.53), and the scaling parameter $\Lambda(\alpha)$ is defined in (2.25). The solid black curve represents the theoretical prediction for the resetting protocol $\psi(\tau) = \frac{\gamma r}{T^\gamma} (T - r\tau)^{\gamma-1}$ for $\tau \in [0, T/r]$, $\gamma = 3$ and $T = 1$. Different symbols correspond to different values of $\alpha = \frac{k}{N}$. Simulations were performed with $N = 10^6$ particles, using $r = 1$ and $D = \frac{1}{2}$.

Importantly, the function $S(z)$ differs from the Gumbel distribution, obtained by sampling N i.i.d. variables from the steady state density (cf. Appendix A.1). It is non-zero over the entire real line and asymptotically behaves as

$$\tilde{S}(z) \approx \begin{cases} \exp[-e^{-z}]\,, & z \to -\infty\,, \\ \exp(-z), & z \to \infty\,. \end{cases} \tag{2.54}$$

In contrast, the resetting-induced distribution is confined to a positive bounded domain. This means that, in the limit $N \to \infty$, the probability that the rightmost particle is at a distance x from the origin is exactly 0 for $x > L\sqrt{T}$ or for $x < 0$. By symmetry, the same distribution also applies to the minimum M_N, up to a change of sign. As a result, the gas is confined within a symmetric region of size $2L\sqrt{T}$ around the origin.

The spacing distribution can be written as

$$\text{Prob}\{d_k = g\} = \frac{1}{\lambda_N(\alpha)} D\left(\frac{g}{\lambda_N(\alpha)}\right) , \tag{2.55}$$

with

$$D(z) = 2\frac{\gamma+1}{T^{\gamma+1}} \int_0^{\sqrt{T}} du \, \left(T - u^2\right)^\gamma \exp\left(-\frac{z}{u}\right) . \tag{2.56}$$

Its asymptotic behaviors are

$$D(z) \approx \begin{cases} B_4 + B_5 z \, \ln z, & z \to 0 \, , \\ B_6 \exp\left(-\frac{z}{\sqrt{T}}\right) , & z \to \infty \, . \end{cases} \tag{2.57}$$

where B_4, B_5 and B_6 are positive constants. Once again, the characteristic length scale is the same as in the Poissonian and power-law cases, reflecting the inherent inhomogeneity of the gas. In the bulk, the typical spacing is $O(1/N)$, while in the tails it is much larger, scaling as $O(1/\sqrt{\ln N})$. A comparison between the theoretical prediction and simulations is shown in Fig. 2.8.

We can now compare our results with those obtained by sampling N i.i.d. variables from the steady-state density, which in this case belongs to the Gumbel class (cf. Appendix A.1). It means that the scaling function $\tilde{D}(z)$ of the distribution of d_1 in the i.i.d. case is given by

$$\tilde{D}(z) = e^{-z} \quad \text{for} \quad z \geq 0 \tag{2.58}$$

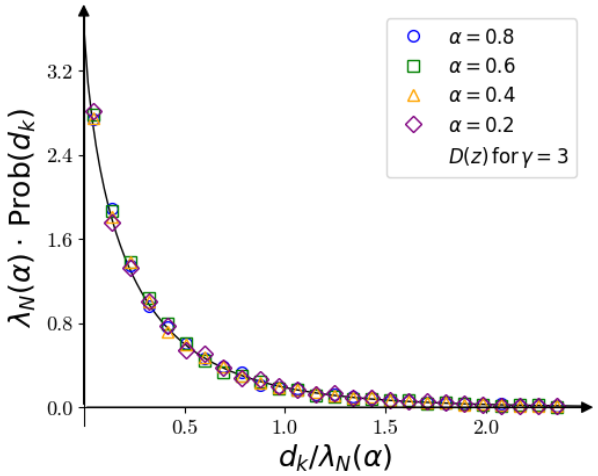

Figure 2.8: Plot of the distribution of the spacing $d_k = M_k - M_{k-1}$ between the k^{th} and $(k-1)^{th}$ rightmost particles. The distribution follows the scaling form $\text{Prob}\{d_k = g\} = \frac{1}{\lambda_N(\alpha)} D\left(\frac{g}{\lambda_N(\alpha)}\right)$, where the scaling function $D(z)$ is given by (2.56), and the scaling parameter $\lambda_N(\alpha)$ is defined in (2.28). The solid black curve represents the theoretical prediction for the resetting protocol $\psi(\tau) = \frac{\gamma r}{T^\gamma}(T - r\tau)^{\gamma-1}$ for $\tau \in [0, T/r]$, $\gamma = 3$ and $T = 1$. Different symbols correspond to different values of $\alpha = \frac{k}{N}$. The simulations were performed with $N = 10^6$ particles, using $r = 1$ and $D = \frac{1}{2}$.

We see that the function (2.58) has the same tail of (2.57) at large z. The small z behavior of (2.57) instead differs from that of (2.58), but it coincides with that found in the two previous cases with $\psi(\tau)$ an exponential or a power-law distribution.
The full counting statistics are obtained via Eq. (2.20), leading to

$$H(k) = \begin{cases} \sigma\sqrt{\pi}\,\dfrac{\gamma+1}{T^{\gamma+1}}\left(T - \dfrac{\sigma}{u(k)^2}\right)^{\gamma} u(k)^{-3}\exp\big(u(k)^2\big)\,, & k > \text{erf}\big(\sqrt{\frac{\sigma}{T}}\big)\,, \\ 0, & k < \text{erf}\big(\sqrt{\frac{\sigma}{T}}\big)\,, \end{cases} \tag{2.59}$$

where $u(k) = \text{erf}^{-1}(k)$ and $\sigma = \frac{rL^2}{4D}$. As $k \to 1^-$, the behavior is

$$H(k) \approx \sigma\sqrt{\pi}\left(\frac{\gamma+1}{T}\right)\frac{1}{(1-k)\,|\ln(1-k)|^{3/2}},$$

which diverges in an integrable manner, exactly as in the Poissonian and power-law cases. In contrast, as $u(k) \to \sqrt{\frac{\sigma}{T}}$ (or equivalently $k \to \text{erf}\big(\sqrt{\frac{\sigma}{T}}\big)$), one finds

$$H(k) \approx \sqrt{\frac{\pi}{\sigma}}\,e^{\frac{\sigma}{T}}\left(\frac{\gamma+1}{T^{\gamma-\frac{1}{2}}}\right)\left(T - \frac{\sigma}{u(k)^2}\right)^{\gamma},$$

which means that, for a fixed box size L, at least a fraction $k = \frac{N_L}{N} = \text{erf}\left(\sqrt{\frac{rL^2}{4DT}}\right)$ of the particles is contained within the box.

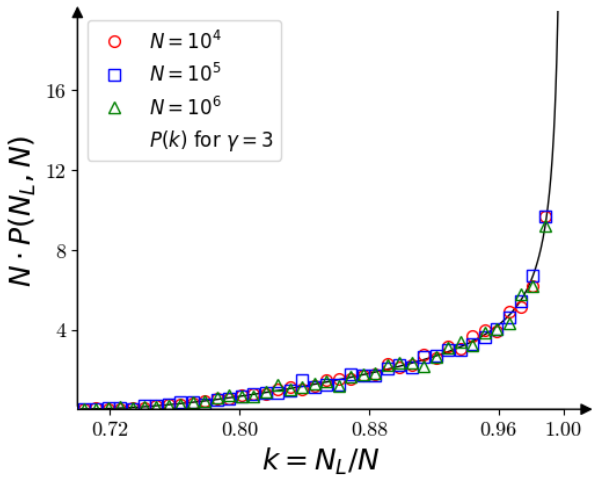

Figure 2.9: Plot of the full counting statistics given by the distribution $P(N_L, N) = \frac{1}{N} H\left(\frac{N_L}{N}\right)$. The scaling function $H(k)$ is given by (2.59). The solid black curve shows the theoretical prediction for the resetting protocol $\psi(\tau) = \frac{\gamma r}{T^\gamma}(T - r\tau)^{\gamma-1}$ for $\tau \in [0, T/r]$, $\gamma = 3$ and $T = 1$. The symbols indicate simulation results for different values of N. The simulations were done with $r = 1$ and $D = \frac{1}{2}$.

Fig. 2.9 shows a comparison between the theoretical prediction and simulation data for different values of N, confirming the expected behavior of $H(k)$.

2.3 Analytical results for general resetting protocols

Thanks to the examples illustrated in Section 2.2, we can now present the general results for the observables in terms of the effective distribution $h(\tau)$. Our main finding is that the scaling function of each observable we have considered is entirely determined by the resetting protocol, which is encoded in the function $h(\tau)$. We identify certain universal features, properties that are independent of the specific form of $h(\tau)$, as well as distinct behaviors arising from different classes of resetting protocols, depending on the asymptotic behavior of $h(\tau)$ at large τ.

First, a characteristic time scale $\frac{1}{r}$ can always be extracted from the resetting distribution $h(\tau)$. Recall that in (2.9) we defined $h(\tau) = r\tilde{h}(r\tau)$, so that $\tilde{h}(z)$ is dimensionless.

Moreover, the observables can be expressed in a specific form due to the c.i.i.d. structure, as shown in (2.12), (2.15), (2.18), and (2.20). This structure allows us to define, for each observable, a corresponding scaling parameter that depends only on the resetting rate r and on the parameters of the propagator, namely, the diffusion constant D and the number of particles N. While the specific scaling parameter varies from one observable to another, it remains the same across different resetting protocols. In this sense, the scaling parameters are universal: they do not depend on the particular form of the resetting distribution.

More concretely:

- The density profile always decays over the length scale

$$l = \sqrt{\frac{D}{r}},$$

regardless of the detailed form of $h(\tau)$.

- The typical distance from the origin of the particle ranked k from the right (i.e., the k^{th} rightmost particle) is

$$\Lambda(\alpha) \;=\; \sqrt{\frac{4D}{r}}\,\mathrm{erfc}^{-1}(2\alpha)\,,$$

where $\alpha = \frac{k}{N}$.

- The mean spacing between successive particles at a certain value α is

$$\lambda_N(\alpha) \;=\; \frac{1}{N\,b\,\sqrt{r}} \quad \text{with} \quad b \;=\; \frac{\exp\!\big(-[\mathrm{erfc}^{-1}(2\alpha)]^2\big)}{\sqrt{4\pi D}}\,.$$

This means that some features of the NESS are completely independent of the resetting protocol. First of all, most particles are confined within a region of size $2l$ about the origin, over which the density decays. In the bulk the particles are very dense, with a typical spacing $\lambda_N(\alpha) \sim O(1/N)$, whereas at the edges the spacing becomes much larger $\lambda_N(\alpha) \sim O(1/\sqrt{\ln N})$. Typically, the particles in the bulk are located at distances $\Lambda(\alpha) \sim O(1)$ from the origin, while the rightmost particle is at a distance of order $\sqrt{\ln N}$. The dependence on the resetting protocol is instead entirely encoded in the scaling functions through the distribution $\tilde{h}(z)$. In fact, the scaling functions for the density $\rho_N(x)$, for the order and extreme value statistics $\mathrm{Prob}\{M_k = \omega\}$, for the gap statistics $\mathrm{Prob}\{d_k = g\}$, and for the full counting statistics $P(N_L, N)$ are given respectively by:

$$R(z) = \frac{1}{\sqrt{\pi}}\int_0^\infty du\,\tilde{h}\big(u^2\big)\exp\!\left(-\frac{z^2}{4u^2}\right), \tag{2.60}$$

$$S(z) = 2z\,\tilde{h}\big(z^2\big), \tag{2.61}$$

$$D(z) = 2\int_0^\infty du\,\tilde{h}\big(u^2\big)\,\exp\!\left(-\frac{z}{u}\right), \tag{2.62}$$

$$H(k) = \sigma\sqrt{\pi}\;u(k)^{-3}\,\exp\big[u(k)^2\big]\;\tilde{h}\Big(\frac{\sigma}{u(k)^2}\Big), \quad \text{with} \quad \sigma = \frac{rL^2}{4D}. \tag{2.63}$$

The first three of these scaling functions exhibit universal behavior at small values of their arguments, while $H(k)$ shows universal behavior as $k \to 1^-$. In fact, from the definition

$$h(\tau = 0) = \frac{\Psi(0)}{\int_0^\infty dt\,\Psi(t)} = \frac{1}{\langle\tau\rangle},$$

we see that as long as the non-equilibrium steady state exists, $h(0)$ is a positive constant, namely the effective resetting rate. As shown in the Appendix A.2, the small-z asymptotics of Eqs. (2.60)–(2.62) simplify to

$$\begin{aligned} R(z) &\approx R_1^0 - R_2^0|z|,\\ S(z) &\approx 2\,\tilde{h}(0)\,z,\\ D(z) &\approx D_1^0 + D_2^0\,z\ln z, \end{aligned}$$

Similarly (see A.2), for the full counting statistics one obtains, as $k \to 1^-$,

$$H(k) \approx H_1^0 \, (1-k)^{-1} \, |\ln(1-k)|^{-3/2},$$

The constants R_1^0, R_2^0, D_1^0, D_2^0 and H_1^0 are positive and their specific value only depend on $h(\tau = 0)$. These results are highly non-trivial, as the z-dependence of all the scaling functions in these regimes never changes and depends solely on the existence of resetting, regardless of the specific form of the resetting protocol.

There are also some universal behaviours at large z (or low k), but, in this case, we have to consider three different universality classes. These classes are defined depending on the tail of $\tilde{h}(y)$ for large y in the following way:

(I) $\tilde{h}(y) \sim e^{-y^\nu}$ for large y.

(II) $\tilde{h}(y) \sim (T-y)^\gamma$, for $y \in [0,T]$ and $\tilde{h}(y) = 0$ outside this domain.

(III) $\tilde{h}(y) \sim y^{-\beta}$ for large y.

We have defined the three classes in this way because of the way in which their asymptotics can be treated (cf. Appendix A.2). For example, in the scaling function of the density (2.60), the integral contains an exponential term. As a result, in the limit $z \to \infty$, the integral is dominated by the large-y behavior of $\tilde{h}(y)$ and we can then substitute the asymptotic form of $\tilde{h}(y)$ into it. In case (I), the integral is dominated by a saddle point; in case (II), the dominant contribution comes from the boundary of the domain at T; in case (III), a simple change of variables is sufficient to evaluate the asymptotics. In this way we get (cf. Appendix A.2):

$$R(z) \approx \begin{cases} R_1^\infty \, z^{\frac{1-\nu}{\nu+1}} \exp\left(-R_2^\infty \, z^{\frac{4\nu}{2\nu+2}}\right) & \text{for type (I)} \\ R_3^\infty \, e^{-\frac{z^2}{4T}} & \text{for type (II)} \\ \frac{R_4^\infty}{z^{2\beta-1}} & \text{for type (III)} \end{cases} \tag{2.64}$$

where R_i^∞ for $i = 1,2,3,4$ are positive constants. We see that in case (I), i.e. when $\tilde{h}(\tau) \sim e^{-\tau^\nu}$ for large τ, the density has also a stretched exponential behavior at large z with an exponent that lies in the interval $(0,2)$: it approaches 0 as ν becomes small and tends to 2 for $\nu \to \infty$. This is interesting since, as we can see, a stretched exponential with an exponent 2 is obtained for (II), i.e. when $\tilde{h}(\tau)$ has a domain bounded from above. This makes sense since a bounded domain $[0,T]$ means that in each time interval T there is for sure at least a resetting event, which is not true when $\psi(\tau)$ is unbounded.

For the function $S(z)$ it is easy to see that $S(z) \approx S_1^\infty \, z \, e^{-z^{2\nu}}$ when $\tilde{h}(y)$ is in class (I), and $S(z) \approx \frac{S_2^\infty}{z^{2\beta-1}}$ for class (III). For the case (II) $S(z)$ has a bounded domain at $z = L\sqrt{T}$. It approaches that point as $S(z) \approx S_3^\infty z (T - z^2)^\gamma$. Since $S(z)$ is the scaling function of both the order statistics and the EVS, the result above implies that the probability of finding the rightmost particle at a distance x from the origin becomes exactly zero in the $N \to \infty$ limit for $x > L\sqrt{T}$ or $x < 0$. Thus, at leading order, the gas is confined within a symmetric region of size $2L\sqrt{T}$ centered around the origin.

Regarding the scaling function of the spacing distribution, since in (2.62) we have an exponential term inside the integral, we find again that the integral is dominated by a saddle point for (I), for (II) it is dominated by the boundary of the domain of $\tilde{h}(y)$ and for (III) we just have to make a change of variable. We obtain (cf. Appendix A.2) respectively that, in the limit of large z:

$$D(z) \approx \begin{cases} D_1^\infty z^{\frac{1-\nu}{2\nu+1}} \exp\left(-D_2^\infty z^{\frac{2\nu}{2\nu+1}}\right) & \text{for type (I)} \\ D_3^\infty e^{-\frac{z}{\sqrt{T}}} & \text{for type (II)} \\ \frac{D_4^\infty}{z^{2\beta-1}} & \text{for type (III)} \end{cases} \tag{2.65}$$

where D_i^∞ for $i = 1, 2, 3, 4$ are positive constants. As before for the density, in case (I) the tail is a stretched exponential with an exponent $\theta = \frac{2\nu}{2\nu+1}$ that this time lies in the interval $(0, 1)$. As for the density, the upper limit $\theta = 1$ is attained for $\nu \to \infty$ and it corresponds to the behavior of $D(z)$ in the case of $\tilde{h}(y)$ of type (II), i.e. with a bounded domain. When instead we are in case (III) we get a power-law tail.

Finally, we recall that the scaling function of the FCS is given by

$$H(k) = \sigma\sqrt{\pi}\, u(k)^{-3} \exp\left[u(k)^2\right] \tilde{h}(y^*)\,, \tag{2.66}$$

having defined

$$u(k) = \mathrm{erf}^{-1}(k), \quad \sigma = \frac{rL^2}{4D}, \quad \text{and} \quad y^* = \frac{\sigma}{u(k)^2}\,.$$

It is evident that, given the dependence of y^* on k, the behavior of $h(\tau)$ for large τ determines that of $H(k)$ for small k. We then obtain that (cf. Appendix A.2):

$$H(k) \approx H^\infty k^{-3} h\left(\frac{4\sigma}{\pi k^2}\right) \tag{2.67}$$

when $k \to 0$. Sobstituting the three possible tails in (2.67) we get

$$H(k) \approx \frac{H_1^\infty}{k^3} \exp\left(-\frac{H_2^\infty}{k^{2\nu}}\right) \quad \text{when } \tilde{h}(y) \text{ is of type (I)}, \tag{2.68}$$

$$H(k) \approx H_3^\infty \left(T - \frac{\sigma}{u(k)^2}\right)^\gamma \quad \text{with a lower bound at } k = \mathrm{erf}\left(\sqrt{\frac{\sigma}{T}}\right) \text{ when } \tilde{h}(y) \text{ is of type (II)}\,, \tag{2.69}$$

$$H(k) \approx H_4^\infty k^{2\beta-3} \quad \text{when } \tilde{h}(y) \text{ is of type (III)}. \tag{2.70}$$

The values H^∞ and H_i^∞ for $i = 1, 2, 3, 4$ are positive constants. The case (II) is particularly interesting since it tells us that, fixed the size of the box L, it contains for sure at least a fraction $k = \frac{N_L}{N} = \mathrm{erf}\left(\sqrt{\frac{rL^2}{4DT}}\right)$ of particles. This reflects the fact that imposing a maximum inter-reset time confines the particles more tightly around the origin than in the other cases.

Conclusions

In this work, we have introduced and analyzed a general class of non-Poissonian resetting protocols for a gas of N independent Brownian particles in one dimension, extending the classical Poissonian case, characterized by the inter-reset time distribution $\psi(\tau) = re^{-r\tau}$, to arbitrary distributions $\psi(\tau)$. While our analysis focused on the one-dimensional case, the approach and main results are easily generalizable to higher-dimensional systems. By exploiting the renewal structure of the dynamics and the concept of conditionally independent and identically distributed (c.i.i.d.) variables, we have characterized the non-equilibrium steady state of the system. This framework enabled the computation of a broad range of observables, including the single-particle density, extreme value statistics, order statistics, gap statistics, and full counting statistics, by expressing them as averages over diffusive processes conditioned on a fixed elapsed time since the last reset. These averages are taken over the distribution $h(\tau) = r\tilde{h}(r\tau)$, which represents the normalized probability of a time interval τ without a reset. While the detailed forms of these observables depend on the specific shape of $\tilde{h}(z)$, their characteristic scales are universal, determined solely by the diffusion coefficient D and the typical reset rate r. We have identified three universality classes based on the tail behavior of $\tilde{h}(z)$: stretched-exponential, power-law, and bounded support. Each class leads to distinct asymptotic forms for the scaling functions associated with the observables studied, namely $R(z)$, $S(z)$, $D(z)$, and $H(k)$, which describe the single-particle density, order and extreme value statistics, gap statistics, and full counting statistics, respectively. Beyond these class-dependent behaviors, we have also found fully universal features in each scaling function, governed solely by the value of $\tilde{h}(0)$. Our theoretical predictions were illustrated and validated numerically through two explicit examples, alongside the classical Poissonian case, each representing one of the universality classes. These results provide a systematic framework to understand and characterize the rich phenomenology arising from non-Poissonian simultaneous resetting of N diffusing particles, offering a class of strongly correlated non-equilibrium systems in which many observables can be computed exactly. This is particularly valuable given that non-equilibrium systems are, in general, poorly understood, and it is often not even possible to compute their steady state. Having a class of models where the steady state is always accessible, and where a wide range of physically measurable observables can be exactly characterized, offers an important opportunity to gain insight into the behavior of out-of-equilibrium systems. Future directions include extending this approach to other many-body systems and to explicit interactions among particles, as resetting can be generalized to arbitrary stochastic processes [36]. Recent experimental realizations of stochastic resetting with colloidal particles [28–31] open the door to exploring the effects of direct interactions in many-body systems under resetting, such as hard-core or hydrodynamic forces.

Bibliography

[1] Martin R. Evans and Satya N. Majumdar. Diffusion with stochastic resetting. *Physical Review Letters*, 106(16), April 2011.

[2] Martin R Evans and Satya N Majumdar. Diffusion with optimal resetting. *Journal of Physics A: Mathematical and Theoretical*, 44(43):435001, October 2011.

[3] Gregorio García-Valladares, Carlos A Plata, Antonio Prados, and Alessandro Manacorda. Optimal resetting strategies for search processes in heterogeneous environments. *New Journal of Physics*, 25(11):113031, November 2023.

[4] Ofir Tal-Friedman, Tommer D. Keidar, Shlomi Reuveni, and Yael Roichman. Smart resetting: An energy-efficient strategy for stochastic search processes, 2024.

[5] Paul C. Bressloff. Search processes with stochastic resetting and multiple targets. *Phys. Rev. E*, 102:022115, Aug 2020.

[6] P. S. Pal, Jong-Min Park, Arnab Pal, Hyunggyu Park, and Jae Sung Lee. Active motion can be beneficial for target search with resetting in a thermal environment. *Phys. Rev. E*, 110:054124, Nov 2024.

[7] Shlomi Reuveni. Optimal stochastic restart renders fluctuations in first passage times universal. *Physical Review Letters*, 116(17), April 2016.

[8] Arnab Pal and Shlomi Reuveni. First passage under restart. *Phys. Rev. Lett.*, 118:030603, Jan 2017.

[9] A. Chechkin and I. M. Sokolov. Random search with resetting: A unified renewal approach. *Phys. Rev. Lett.*, 121:050601, Aug 2018.

[10] Arnab Pal, Łukasz Kuśmierz, and Shlomi Reuveni. Search with home returns provides advantage under high uncertainty. *Physical Review Research*, 2(4), November 2020.

[11] Ross G. Pinsky. Diffusive search with spatially dependent resetting, 2018.

[12] Benjamin De Bruyne, Satya N. Majumdar, and Grégory Schehr. Optimal resetting brownian bridges via enhanced fluctuations. *Phys. Rev. Lett.*, 128:200603, May 2022.

[13] Urna Basu, Sanjib Sabhapandit, and Ion Santra. *Target Search by Active Particles*, page 463–487. Springer Nature Switzerland, 2024.

[14] Marco Biroli, Satya N. Majumdar, and Grégory Schehr. Critical number of walkers for diffusive search processes with resetting. *Phys. Rev. E*, 107:064141, Jun 2023.

[15] Arnab Pal, Anupam Kundu, and Martin R Evans. Diffusion under time-dependent resetting. *Journal of Physics A: Mathematical and Theoretical*, 49(22):225001, April 2016.

[16] Ofir Blumer, Shlomi Reuveni, and Barak Hirshberg. Stochastic resetting for enhanced sampling. *The Journal of Physical Chemistry Letters*, 13(48):11230–11236, November 2022.

[17] Manuel Villén-Altamirano and José Villén-Altamirano. Restart: A method for accelerating rare event simulations. 3, 01 1991.

[18] Michael Luby, Alistair Sinclair, and David Zuckerman. Optimal speedup of las vegas algorithms. *Information Processing Letters*, 47:173–180, 04 1997.

[19] Hanghang Tong, Christos Faloutsos, and Jia-Yu Pan. Random walk with restart: fast solutions and applications. *Knowledge and Information Systems*, 14(3):327–346, 2008.

[20] Konstantin Avrachenkov, Alexei Piunovskiy, and Zhang Yi. Markov processes with restart, 2012.

[21] Jan-Hendrik Lorenz. *Runtime Distributions and Criteria for Restarts*, page 493–507. Springer International Publishing, December 2017.

[22] Édgar Roldán, Ana Lisica, Daniel Sánchez-Taltavull, and Stephan W. Grill. Stochastic resetting in backtrack recovery by rna polymerases. *Physical Review E*, 93(6), June 2016.

[23] Ana Lisica, Christoph Engel, Marcus Jahnel, Édgar Roldán, Eric A. Galburt, Patrick Cramer, and Stephan W. Grill. Mechanisms of backtrack recovery by rna polymerases i and ii. *Proceedings of the National Academy of Sciences of the United States of America*, 113(11):2946–2951, 2016.

[24] Martin R Evans and Satya N Majumdar. Run and tumble particle under resetting: a renewal approach. *Journal of Physics A: Mathematical and Theoretical*, 51(47):475003, October 2018.

[25] A. Scacchi and A. Sharma. Mean first passage time of active brownian particle in one dimension. *Molecular Physics*, 116(4):460–464, December 2017.

[26] Lukasz Kusmierz, Satya N. Majumdar, Sanjib Sabhapandit, and Grégory Schehr. First order transition for the optimal search time of lévy flights with resetting. *Phys. Rev. Lett.*, 113:220602, Nov 2014.

[27] Tian Zhou, Pengbo Xu, and Weihua Deng. Continuous-time random walks and lévy walks with stochastic resetting. *Physical Review Research*, 2(1), January 2020.

[28] Benjamin Besga, Alfred Bovon, Artyom Petrosyan, Satya N. Majumdar, and Sergio Ciliberto. Optimal mean first-passage time for a brownian searcher subjected to resetting: Experimental and theoretical results. *Physical Review Research*, 2(3), July 2020.

[29] F Faisant, B Besga, A Petrosyan, S Ciliberto, and Satya N Majumdar. Optimal mean first-passage time of a brownian searcher with resetting in one and two dimensions: experiments, theory and numerical tests. *Journal of Statistical Mechanics: Theory and Experiment*, 2021(11), 2021.

[30] Ofir Tal-Friedman, Arnab Pal, Amandeep Sekhon, Shlomi Reuveni, and Yael Roichman. Experimental realization of diffusion with stochastic resetting. *The Journal of Physical Chemistry Letters*, 11(17):7350–7355, August 2020.

[31] Ron Vatash and Yael Roichman. Many-body colloidal dynamics under stochastic resetting: Competing effects of particle interactions on the steady state distribution, 2025.

[32] B. Mukherjee, K. Sengupta, and Satya N. Majumdar. Quantum dynamics with stochastic reset. *Physical Review B*, 98(10), September 2018.

[33] Dominic C. Rose, Hugo Touchette, Igor Lesanovsky, and Juan P. Garrahan. Spectral properties of simple classical and quantum reset processes. *Physical Review E*, 98(2), August 2018.

[34] Sascha Wald, Louie Hong Yao, Thierry Platini, Chris Hooley, and Federico Carollo. Stochastic resetting in discrete-time quantum dynamics: steady states and correlations in few-qubit systems, 2024.

[35] Ashutosh Kumar, Sourabh Lahiri, Trilochan Bagarti, and Subhashish Banerjee. Two and three-state quantum heat engines with stochastic resetting, 2025.

[36] Martin R Evans, Satya N Majumdar, and Grégory Schehr. Stochastic resetting and applications. *Journal of Physics A: Mathematical and Theoretical*, 53(19):193001, April 2020.

[37] Apoorva Nagar and Shamik Gupta. Diffusion with stochastic resetting at power-law times. *Physical Review E*, 93(6), June 2016.

[38] Stephan Eule and Jakob J Metzger. Non-equilibrium steady states of stochastic processes with intermittent resetting. *New Journal of Physics*, 18(3):033006, March 2016.

[39] Marco Biroli, Hernan Larralde, Satya N. Majumdar, and Grégory Schehr. Extreme statistics and spacing distribution in a brownian gas correlated by resetting. *Physical Review Letters*, 130(20), May 2023.

[40] Marco Biroli, Hernán Larralde, Satya N. Majumdar, and Grégory Schehr. Exact extreme, order, and sum statistics in a class of strongly correlated systems. *Physical Review E*, 109(1), January 2024.

[41] Matteo Magoni, Satya N. Majumdar, and Grégory Schehr. Ising model with stochastic resetting. *Physical Review Research*, 2(3), August 2020.

[42] Marco Biroli, Manas Kulkarni, Satya N. Majumdar, and Grégory Schehr. Dynamically emergent correlations between particles in a switching harmonic trap. *Physical Review E*, 109(3), March 2024.

[43] Shamik Gupta, Satya N. Majumdar, and Grégory Schehr. Fluctuating interfaces subject to stochastic resetting. *Phys. Rev. Lett.*, 112:220601, Jun 2014.

[44] B.C. Arnold, N. Balakrishnan, and H.N. Nagaraja. *A First Course in Order Statistics*. Wiley, New York, 1992.

[45] H.N. Nagaraja and H.A. David. *Order Statistics*. Wiley, New Jersey, 3rd edition, 2003.

[46] Satya N. Majumdar, Arnab Pal, and Grégory Schehr. Extreme value statistics of correlated random variables: A pedagogical review. *Physics Reports*, 840:1–32, January 2020.

[47] Satya N Majumdar and Grégory Schehr. *Statistics of Extremes and Records in Random Sequences*. Oxford University Press, 06 2024.

[48] I. Weissman. 2. a survey of results on extremes of independent non-identically distributed random variables. *Advances in Applied Probability*, 20(1):8–8, 1988.

[49] Gregory Schehr and Satya N. Majumdar. Exact record and order statistics of random walks via first-passage ideas, 2013.

Appendix A

A.1 EVS for i.i.d. variables

We briefly summarize some classical results concerning the statistics of extremes for independent and identically distributed (i.i.d.) random variables. Let $\{x_1, x_2, \ldots, x_N\}$ be i.i.d. random variables drawn from a PDF $p(x)$, and let their ordered values be denoted as $\{M_1 > M_2 > \ldots > M_N\}$. This problem is well studied in the literature [44–47].

According to the Fisher–Tippett–Gnedenko theorem, in the limit $N \to \infty$, the distribution $\text{Prob}\{M_1 = \omega\}$, when properly centered and rescaled, converges to one of three universal forms:

$$\text{Prob}\{M_1 = a_N + b_N z\} \xrightarrow{N\to\infty} f_\rho(z), \tag{A.1}$$

where $\rho = I, II, III$ indicates the three classes. The scaling factors a_N and b_N depend on the parent distribution $p(x)$, while the scaling function $f_\rho(z)$ is universal, determined solely by the tail behavior of $p(x)$. The three universality classes are:

1. **Gumbel (Class I):** When $p(x)$ decays faster than any power law on an unbounded domain, the limiting form is the Gumbel distribution:

$$f_I(z) = e^{-z-e^{-z}}.$$

2. **Fréchet (Class II):** When $p(x) \sim x^{-1-\alpha}$ for large x (heavy-tailed), the limiting distribution is:

$$f_{II}(z) = \frac{\alpha}{z^{1+\alpha}} e^{-z^{-\alpha}}, \quad z > 0.$$

3. **Weibull (Class III):** When $p(x)$ has bounded support, i.e., $p(x) \sim B(a-x)^{\gamma-1}$ for $x \leq a$, the distribution becomes:

$$f_{III}(z) = \gamma(-z)^{\gamma-1} e^{-(-z)^\gamma}, \quad z < 0.$$

For M_k with $k = O(1)$, a similar result holds: the scaling function of the rescaled variable $z = \frac{M_k - a_N}{b_N}$ depends on k, but a_N and b_N remain the same as for $k = 1$.

Likewise, the statistics of the gaps $d_k = M_k - M_{k+1}$ obey the scaling form [44–47]:

$$\text{Prob}\{d_k = b_N z\} \xrightarrow{N\to\infty} \tilde{p}_{k,\rho}(z),$$

with the following asymptotic distributions:

1. **Gumbel (Class I):**
$$\tilde{p}_{k,I}(z) = \Theta(z)\, k e^{-kz}$$

2. **Fréchet (Class II):**
$$\tilde{p}_{k,II}(z) = \Theta(z)\, \frac{\alpha^2}{(k-1)!} \int_0^\infty e^{-x^{-\alpha}} x^{-\alpha-1} (x+z)^{-\alpha k-1}\, dx$$

3. **Weibull (Class III):**
$$\tilde{p}_{k,III}(z) = \Theta(z)\, \frac{\gamma^2}{(k-1)!} \int_0^\infty (x+z)^{\gamma-1} e^{-(x+z)^\gamma} x^{\gamma k-1}\, dx$$

These results are valid for $k \geq 1$, provided $k = O(1)$.

A.2 Derivations of some analytical results

In this subsection, we derive general results for the scaling functions of the observables considered in the main text.

A.2.1 Small z behaviour for $R(z)$, $D(z)$, $S(z)$

We start by recalling that, as long as the non-equilibrium steady state exists, $h(0)$ is a positive constant.

Density profile $R(z)$

The density of particles can be written in the scaling form
$$\rho_N(x) = \frac{1}{l} R\left(\frac{x}{l}\right), \tag{A.2}$$

where $l = \sqrt{\frac{D}{r}}$, and
$$R(z) = \frac{1}{\sqrt{\pi}} \int_0^\infty \mathrm{d}u\, \tilde{h}(u^2) \exp\left(-\frac{z^2}{4u^2}\right). \tag{A.3}$$

We aim to show that, since $\tilde{h}(0)$ is a non-zero value, the small-z behavior of $R(z)$ is
$$R(z) \approx R_1^0 - R_2^0 |z|,$$

A direct expansion of (A.3) is not effective, so we consider instead its derivative:
$$R'(z) = \frac{dR(z)}{dz} = -\frac{2z}{\sqrt{\pi}} \int_0^\infty \mathrm{d}u\, \frac{\tilde{h}(u^2)}{u^2} \exp\left(-\frac{z^2}{4u^2}\right). \tag{A.4}$$

Performing the change of variables $y = z/u$, we obtain
$$R'(z) = -\frac{2}{\sqrt{\pi}} \int_0^\infty \mathrm{d}y\, \tilde{h}\left(\frac{z^2}{y^2}\right) \exp\left(-\frac{y^2}{4}\right). \tag{A.5}$$

In the limit $z \to 0$, the argument of $\tilde{h}$ tends to zero, so we can approximate $\tilde{h}(z^2/y^2) \approx \tilde{h}(0)$. Thus,

$$R'(z) \xrightarrow{z\to 0} -\frac{2\tilde{h}(0)}{\sqrt{\pi}} \int_0^\infty \mathrm{d}y \, \exp\left(-\frac{y^2}{4}\right),$$

which is a finite constant. This implies that $R(z) \approx R_1^0 - R_2^0|z|$ for small z, consistently with the even symmetry of the density profile.

The constants R_1^0 and R_2^0 are given by

$$R_1^0 = R(0) = \frac{1}{\sqrt{\pi}} \int_0^\infty \mathrm{d}u \, \tilde{h}(u^2), \qquad R_2^0 = \frac{2\tilde{h}(0)}{\sqrt{\pi}} \int_0^\infty \mathrm{d}y \, \exp\left(-\frac{y^2}{4}\right) = 2\tilde{h}(0). \tag{A.6}$$

Gap statistics $D(z)$

We now consider the scaling function associated with the spacing distribution:

$$D(z) = 2 \int_0^\infty \mathrm{d}u \, \tilde{h}(u^2) \exp\left(-\frac{z}{u}\right). \tag{A.7}$$

We can reason as we have done above for $R(z)$: we consider the derivative $D'(z)$ and perform the change of variable $y = \frac{z}{u}$ inside the integral. This leads to

$$D'(z) \approx -\int_z^\infty dy \, \frac{e^{-y}}{y} \, \tilde{h}\left(\frac{z^2}{y^2}\right) \tag{A.8}$$

As $z \to 0$ we can set $\tilde{h}\left(\frac{z^2}{y^2}\right) = \tilde{h}(0)$ and perform an integration by parts. This leads to $D'(z) \propto \ln z$ and, after another integration, to

$$D(z) \approx D_1^0 + D_2^0 \, z \ln z,$$

Order and extreme value statistics $S(z)$

In this case the scaling function is $S(z) = 2z\,\tilde{h}(z^2)$. This trivially gives $S(z) \xrightarrow{z\to 0} 2\tilde{h}(0)z$, which is a linear behavior independent of the reset protocol except for its value in the origin.

A.2.2 Large z behaviour for $R(z)$, $D(z)$, $S(z)$

We now study the large-z behavior of $R(z)$, $D(z)$, $S(z)$ for the three universality classes defined as

(I) $\tilde{h}(y) \sim e^{-y^\nu}$ for large y.

(II) $\tilde{h}(y) \sim (T-y)^\gamma$, for $y \in [0, T]$ and $\tilde{h}(y) = 0$ outside this domain.

(III) $\tilde{h}(y) \sim y^{-\beta}$ for large y.

For the first case (I), in the limit $z \to \infty$, the integral in (A.3) is dominated by large u. Substituting the asymptotic form, we write

$$R(z) \approx \frac{1}{\sqrt{\pi}} \int_0^\infty \mathrm{d}u \, \exp\left[-f(u)\right], \quad \text{with} \quad f(u) = u^{2\nu} + \frac{z^2}{4u^2}.$$

To apply the saddle point method we notice that the minimum of $f(u)$ occurs at

$$u^* = \left(\frac{z^2}{4\nu}\right)^{1/(2\nu+2)}.$$

Expanding up to the second order $f(u)$ around this point and then performing a Gaussian integral gives the leading behavior

$$R(z) \approx R_1^\infty \, z^{\frac{1-\nu}{\nu+1}} \exp\left(-R_2^\infty \, z^{\frac{4\nu}{2\nu+2}}\right), \tag{A.9}$$

where R_1^∞ and R_2^∞ are positive constants depending only on ν.

Using the same procedure, we find that for large z,

$$D(z) \approx D_1^\infty \, z^{\frac{1-\nu}{2\nu+1}} \exp\left(-D_2^\infty \, z^{\frac{2\nu}{2\nu+1}}\right), \tag{A.10}$$

with positive constants D_1^∞ and D_2^∞.

When instead we are in case (II), the integrals defining $R(z)$ and $D(z)$ are given by

$$R(z) = \frac{1}{\sqrt{\pi}} \int_0^{\sqrt{T}} \mathrm{d}u \, \tilde{h}(u^2) \exp\left(-\frac{z^2}{4u^2}\right) \tag{A.11}$$

$$D(z) = 2 \int_0^{\sqrt{T}} \mathrm{d}u \, \tilde{h}(u^2) \exp\left(-\frac{z}{u}\right) \tag{A.12}$$

For large z they are dominated by the boundary $u \sim \sqrt{T}$. This suggests that we can substitute the tail (II) of $\tilde{h}(y)$ and perform the change of variable $u = \sqrt{T(1-\epsilon)}$. It leads to

$$R(z) = \sqrt{\frac{T}{\pi}} \int_0^1 \mathrm{d}\epsilon \, \left(T - T(1-\epsilon)^2\right)^\gamma \exp\left(-\frac{z^2}{4T(1-\epsilon)^2}\right) \tag{A.13}$$

$$D(z) = 2\sqrt{T} \int_0^1 \mathrm{d}\epsilon \, \left(T - T(1-\epsilon)^2\right)^\gamma \exp\left(-\frac{z}{\sqrt{T}(1-\epsilon)}\right) \tag{A.14}$$

For $z \to \infty$ only the values $\epsilon \sim 0$ will matter and we can further approximate $u^2 = T(1-\epsilon)^2 \approx T(1-2\epsilon)$, $1/u^2 \approx \frac{1+2\epsilon}{T}$ and $1/u \approx \frac{1+\epsilon}{\sqrt{T}}$. We obtain

$$R(z) = \sqrt{\frac{T}{\pi}} (2T)^\gamma e^{-\frac{z^2}{4T}} \int_0^1 \mathrm{d}\epsilon \, \epsilon^\gamma \exp\left(-\frac{z^2}{2T}\epsilon\right) = \sqrt{\frac{T}{\pi}} \frac{(2T)^\gamma}{\gamma+1} e^{-\frac{z^2}{4T}} \tag{A.15}$$

$$D(z) = 2\sqrt{T}(2T)^\gamma e^{-\frac{z}{\sqrt{T}}} \int_0^1 \mathrm{d}\epsilon \, \epsilon^\gamma \exp\left(-\frac{z}{\sqrt{T}}\epsilon\right) = \frac{2\sqrt{T}(2T)^\gamma}{\gamma+1} e^{-\frac{z}{\sqrt{T}}} \tag{A.16}$$

where we have used that

$$\lim_{z\to 0} \int_0^1 x^\gamma e^{-a\,x\,z^\alpha} \, dx = \frac{1}{1+\gamma} \quad \forall\, a > 0, \gamma > -1, \quad \text{for} \quad \alpha = 1, 2 \tag{A.17}$$

We now consider class (III), i.e. $\tilde{h}(y) \sim y^{-\beta}$ when y is large. When $z \to \infty$ the scaling functions $R(z)$ and $D(z)$ are again dominated by large values of u in the integration domain. We can then sobstitute the tail of $\tilde{h}$ in (2.60) and (2.62) to get

$$R(z) = \frac{1}{\sqrt{\pi}} \int_0^\infty \mathrm{d}u \, \frac{1}{u^{2\beta}} \exp\left(-\frac{z^2}{4u^2}\right) \tag{A.18}$$

$$D(z) = 2 \int_0^\infty \mathrm{d}u \, \frac{1}{u^{2\beta}} \exp\left(-\frac{z}{u}\right) \tag{A.19}$$

Making the change of variable $\frac{z}{u} = y$, and using the relation $\int_0^\infty dy\, y^{2\beta-2} e^{-y^2} = \frac{1}{2}\Gamma(\beta - \frac{1}{2})$, where $\Gamma(x)$ is the gamma function defined by $\Gamma(x) = \int_0^\infty dy\, y^{x-1}\, e^{-y}$. This gives us

$$R(z) = \frac{2^{2\beta-2}\Gamma(\beta - \frac{1}{2})}{\sqrt{\pi}} \frac{1}{z^{2\beta-1}} \tag{A.20}$$

$$D(z) = \frac{\Gamma\left(\beta - \frac{1}{2}\right)}{z^{2\beta-1}} \tag{A.21}$$

This expansion is valid as long as $\beta > \frac{1}{2}$, but we can only consider $\beta > 1$ in order to have a stationary state.

The $z \to \infty$ behaviour of $S(z)$ is instead trivial, one just needs to insert the three possible tails in the expression $S(z) = 2\, z\, \tilde{h}(z)$.

A.2.3 Asymptotics for the FCS $H(k)$

The function $H(k)$ is defined as

$$H(k) = \sigma\sqrt{\pi}\, u(k)^{-3} \exp\left(u(k)^2\right) \tilde{h}(\tau^*), \tag{A.22}$$

where $u(k) = \mathrm{erf}^{-1}(k)$, and $\tau^* = \sigma/u(k)^2$ with $\sigma = \frac{rL^2}{4D}$.

As $k \to 1^-$, the inverse error function diverges logarithmically:

$$u(k) \sim \sqrt{-\ln(1-k)}. \tag{A.23}$$

This implies $\tau^* \to 0$, and thus $\tilde{h}(\tau^*) \to \tilde{h}(0)$. Substituting (A.23) into (A.22), we find

$$H(k) \approx H_1^0\, (1-k)^{-1} |\ln(1-k)|^{-3/2}, \tag{A.24}$$

with $H_1^0 \propto \tilde{h}(0)$.

In the opposite limit $k \to 0$, we use the expansion $u(k) \sim \frac{\sqrt{\pi}}{2} k$. This results in

$$\tau^* \sim \frac{4\sigma}{\pi k^2}, \quad u(k)^3 \sim k^3, \quad \text{and} \quad \exp(u(k)^2) \sim 1$$

From (A.22) we then obtain

$$H(k) \approx H^\infty\, k^{-3} \tilde{h}\left(\frac{4\sigma}{\pi k^2}\right), \tag{A.25}$$

where H^∞ is a positive constant.